© 2022. Published by The Company of Biologists Ltd | Development (2022) 149, dev200133. doi:10.1242/dev.200133

STEM CELLS AND REGENERATION

TECHNIQUES AND RESOURCES ARTICLE

Identification of enhancer regulatory elements that direct epicardial gene expression during zebrafish heart regeneration

Yingxi Cao[1,2], Yu Xia[1,2], Joseph J. Balowski[3,4], Jianhong Ou[3,4], Lingyun Song[5,6], Alexias Safi[5,6], Timothy Curtis[3,4], Gregory E. Crawford[5,6], Kenneth D. Poss[3,4,*] and Jingli Cao[1,2,*]

ABSTRACT

The epicardium is a mesothelial tissue layer that envelops the heart. Cardiac injury activates dynamic gene expression programs in epicardial tissue, which in zebrafish enables subsequent regeneration through paracrine and vascularizing effects. To identify tissue regeneration enhancer elements (TREEs) that control injury-induced epicardial gene expression during heart regeneration, we profiled transcriptomes and chromatin accessibility in epicardial cells purified from regenerating zebrafish hearts. We identified hundreds of candidate TREEs, which are defined by increased chromatin accessibility of non-coding elements near genes with increased expression during regeneration. Several of these candidate TREEs were incorporated into stable transgenic lines, with five out of six elements directing injury-induced epicardial expression but not ontogenetic epicardial expression in larval hearts. Whereas two independent TREEs linked to the gene *gnai3* showed similar functional features of gene regulation in transgenic lines, two independent *ncam1a*-linked TREEs directed distinct spatiotemporal domains of epicardial gene expression. Thus, multiple TREEs linked to a regeneration gene can possess either matching or complementary regulatory controls. Our study provides a new resource and principles for understanding the regulation of epicardial genetic programs during heart regeneration.

This article has an associated 'The people behind the papers' interview.

KEY WORDS: Epicardium, Enhancer, TREE, Heart regeneration, Zebrafish, ATAC-seq

INTRODUCTION

The zebrafish heart is capable of complete or near-complete regeneration after injury, based on proliferation of spared cardiomyocytes (CMs) (Poss et al., 2002). The pro-regenerative environment provided by non-muscle cells, such as the epicardium, endocardium, vasculature and immune cells, contributes to this potential (Cao and Poss, 2018; Gemberling et al., 2015; Gonzalez-Rosa et al., 2012; Hui et al., 2017; Karra et al., 2018; Kikuchi et al., 2011a; Lepilina et al., 2006; Masters and Riley, 2014; Wang et al., 2013). For example, genetic ablation of the epicardium, a thin mesothelial layer that envelops all vertebrate hearts, blocks heart muscle regeneration and coronary angiogenesis in zebrafish (Wang et al., 2015). Key developmentally potent genes, such as retinaldehyde dehydrogenase 2 (*raldh2*), T-box transcription factor 18 (*tbx18*), fibronectin 1 (*fn1*) and neuregulin 1 (*nrg1*), are induced in epicardial tissue upon cardiac injury, first organ-wide and then resolving to the site of trauma (Fig. 1A), in a phenomenon known as 'epicardial activation' (Gemberling et al., 2015; Lepilina et al., 2006; Wang et al., 2013). Understanding the gene expression responses to injury that define epicardial activation can illuminate defining aspects of heart regeneration (Cao and Poss, 2018).

Enhancers are a class of cis-regulatory elements that help orchestrate gene expression during animal development and in response to environmental changes (Pennacchio et al., 2013). Kang et al. first reported a short non-coding DNA sequence upstream of the gene *leptin b* (*lepb*) that can direct expression in zebrafish hearts and fins upon injury and during regeneration, referring to these context-preferential sequences as tissue regeneration enhancer elements (TREEs). TREEs can be identified by comparing profiles of chromatin structure or decorations from uninjured and regenerating tissues. From these profiles, sequences near genes that increase RNA levels during regeneration, and in which increased marks of activated enhancers are evident in the regeneration contexts, represent candidate TREEs. Generation of transgenic animals and/or mutant animals is essential to validate TREEs, which have been described and validated in many contexts, including zebrafish hearts, zebrafish and killifish fins, and *Drosophila* imaginal discs (Begeman et al., 2020; Goldman et al., 2017; Harris et al., 2016; Kang et al., 2016; Pfefferli and Jazwinska, 2017; Wang et al., 2020). The discovery of specific regulatory sequences that underlie regeneration programs can reveal candidate upstream and downstream factors in regeneration, while also providing tools with which to manipulate regeneration (Chen et al., 2020; Kang et al., 2016; Sugimoto et al., 2017; van Duijvenboden et al., 2019).

Initial studies have made it clear that different cell populations engage distinct compendia of TREEs during their respective regenerative responses (Goldman et al., 2017; Lee et al., 2020; Thompson et al., 2020; Vizcaya-Molina et al., 2018). Here, to elucidate candidate TREEs responsible for epicardial gene expression responses, we profiled the chromatin accessibility of epicardial cells during heart regeneration in zebrafish by ATAC-seq (Buenrostro et al., 2013), validating several candidate TREEs using stable transgenic reporter lines. Our study provides a resource of gene regulatory changes in epicardial cells during heart regeneration and reveals new concepts in TREE-based gene regulation.

[1]Cardiovascular Research Institute, Weill Cornell Medicine, 1300 York Avenue, New York, NY 10021, USA. [2]Department of Cell and Developmental Biology, Weill Cornell Medicine, 1300 York Avenue, New York, NY 10021, USA. [3]Department of Cell Biology, Duke University Medical Center, Durham, NC 27710, USA. [4]Duke Regeneration Center, Duke University, Durham, NC 27710, USA. [5]Center for Genomic and Computational Biology, Duke University Medical Center, Durham, NC 27710, USA. [6]Department of Pediatrics, Division of Medical Genetics, Duke University Medical Center, Durham, NC 27710, USA.

*Authors for correspondence (ken.poss@duke.edu; jic4001@med.cornell.edu)

J.C., 0000-0001-5938-6604; J.O., 0000-0002-8652-2488

Handling Editor: Steve Wilson
Received 23 August 2021; Accepted 11 January 2022

Development (2022) 149, dev200133. doi:10.1242/dev.200133

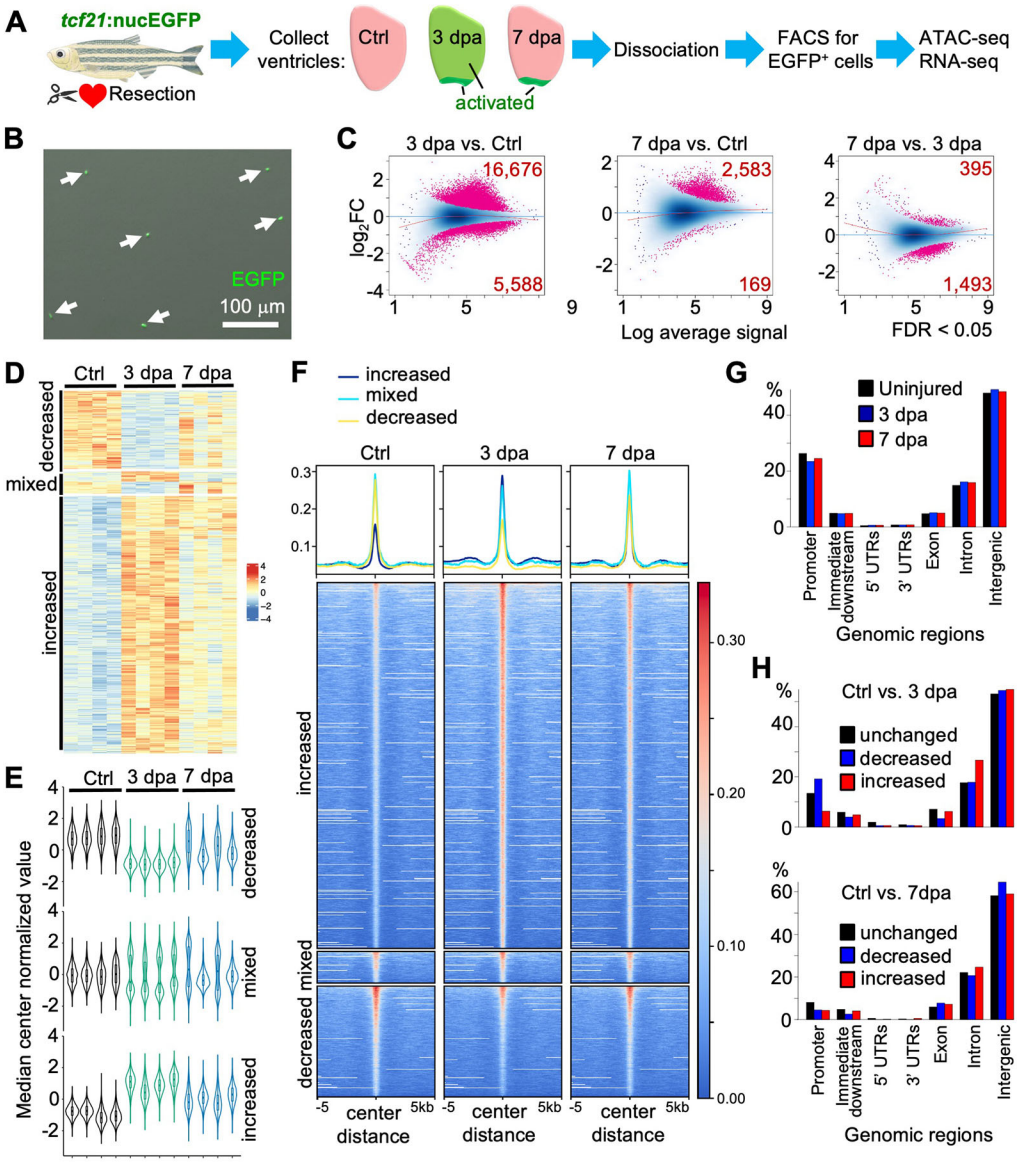

Fig. 1. ATAC-seq analysis reveals dynamic chromatin accessibility in epicardial cells during heart regeneration. (A) Schematic for experimental design. Partial resection injuries were carried out in *tcf21:nucEGFP* animals. Ventricles were collected at 3 or 7 dpa, as were those of uninjured clutchmates (Ctrl). Areas of epicardial activation are labeled in green. Ventricles were dissociated, EGFP$^+$ epicardial cells were isolated by FACS, and bulk RNA-seq and ATAC-seq were performed. (B) FACS-isolated cells in a culture dish to examine survival, morphology and EGFP signals. Arrows indicate EGFP$^+$ cells. (C) MA plots of Log_2 fold changes (Log_2FC) over average normalized ATAC-seq signals. Pink dots indicate peaks with significantly changed chromatin accessibility with the numbers of differential peaks labeled in the corners (FDR<0.05). (D) Heat map of differential chromatin accessibility across three groups with four replicates each. Three clusters (increased, mixed and decreased) are indicated on the left. Increased, peaks with increased accessibility in both 3 and 7 dpa samples; decreased, peaks with decreased chromatin accessibility in both 3 and 7 dpa samples compared with the uninjured control; mixed, peaks with different trends in 3 and 7 dpa samples, compared with the control. (E) Violin plots of differential peaks of three clusters across samples, showing the distribution pattern of chromatin accessibility across samples. (F) Heat map shows the signals of ATAC-seq within ±5 kb of the peak centers. The blue, cyan and yellow lines at the top represent mean read densities of the corresponding ATAC-seq peaks at increased, mixed and decreased chromatin accessibility, respectively. (G) Genomic distributions of all ATAC-seq peaks in three groups. (H) Genomic distributions of the differential and unchanged regions in pair-wise comparisons (top, 3 dpa versus Ctrl; bottom, 7 dpa versus Ctrl).

RESULTS

ATAC-seq analysis of epicardial chromatin structure during heart regeneration

To identify candidate TREEs that direct epicardial gene expression, we profiled transcriptomes and whole-genome chromatin accessibility by bulk RNA-seq and ATAC-seq from purified epicardial cells. We postulated that these datasets would reveal areas of active regulation, including enhancer elements linked to genes involved in epicardial responses to injury and regeneration. To isolate epicardial cells, we used an EGFP reporter driven by the regulatory sequences of *tcf21*. Although epicardial cells are a heterogeneous population and *tcf21* conceivably does not label the entire population, it is the best available pan-epicardial marker that labels both quiescent and injury-responding epicardial cells in zebrafish (Cao et al., 2016; Kikuchi et al., 2011a; Weinberger et al., 2020). To elicit a strong epicardial injury response, we performed ventricular resection injuries on *tcf21:nucEGFP* animals and collected ventricles at 3 and 7 days post-

Development (2022) 149, dev200133. doi:10.1242/dev.200133

amputation (dpa) together with uninjured ventricles (Ctrl) and isolated EGFP$^+$ cells at >95% purity (Fig. 1A,B). These two time-points represent a stage of organ-wide epicardial activation (3 dpa) and injury site-restricted activation (7 dpa, Fig. 1A) (Lepilina et al., 2006). From four biological replicates, we identified 315,000 open chromatin sites on average in each experimental group (Table S1). In 3 dpa samples, 16,676 sites displayed increased chromatin accessibility compared with samples from uninjured hearts, whereas 5588 had decreased accessibility [Fig. 1C and Table S2, false discovery rate (FDR) <0.05]. By 7 dpa, chromatin accessibility appeared to largely normalize: 2583 sites had significantly increased chromatin accessibility and 169 sites had decreased accessibility (Fig. 1C). Clustering of these differential sites across samples derived three clusters with distinct changes in chromatin accessibility. The first cluster displayed increased accessibility during regeneration in both 3 and 7 dpa samples (Fig. 1D-F, increased), while the second cluster showed reduced accessibility (Fig. 1D-F, decreased). The last cluster has mixed trends (increased or decreased) in 3 and 7 dpa samples, with the 7 dpa sample more similar to the control (Fig. 1D-F, mixed). We next analyzed peak distribution by genomic region. In all three experimental groups, about 25% of the peaks resided in promoters, ∼15% in introns, ∼5% in exons and ∼50% are intergenic. The rest are within the untranslated regions (UTRs) and immediate downstream regions (Fig. 1G). The increased regions at 3 dpa (versus Ctrl) mostly resided in the intergenic (∼55%) and intronic regions (∼25%) (Fig. 1H). Together, these results suggest that there is substantial chromatin remodeling in epicardial cells after injury, and this remodeling is more extreme at 3 dpa than at 7 dpa.

To more closely examine these data for active regulatory elements, we integrated our ATAC-seq dataset with the published histone H3K27Ac (H3 acetylation at lysine 27) signature captured from regenerating zebrafish ventricles (Kang et al., 2016). This dataset comprises profiles of two biological replicates of ventricles regenerating after partial genetic ablation of CMs (regenerating) and uninjured ventricles (control). We examined trends of differential ATAC peaks, finding that regions with either increased or decreased accessibility during regeneration bear H3K27Ac signatures in whole-ventricle samples (Fig. 2A). However, only those regions with increased accessibility correlate well with a signature of increased H3K27Ac marks in regenerating samples (Fig. 2B, regenerating/control ratio >1). By contrast, those regions decreasing do not show changes in the H3K27Ac signature (Fig. 2B, bottom, ratio=1). This analysis implicates regions of DNA with increased chromatin accessibility in epicardial cells during heart regeneration as candidate TREEs. As an example, Fig. 2C shows the genomic region that contains Wilms tumor 1 transcription factor b (*wt1b*), a key epicardial transcription factor induced by injury in zebrafish (Kikuchi et al., 2011a). Four peaks upstream (−13 kb, −19 kb, −20 kb and −24 kb) of the transcription start site (TSS) of *wt1b* demonstrated increased accessibility at both 3 and 7 dpa. Three of these peaks have increased H3K27Ac marks in the regenerating ventricle dataset (peaks 1-3). Similarly, ATAC-seq peaks with increased accessibility are observed in the genomic regions that contain aldehyde dehydrogenase 1 family, member A2 [*aldh1a2*, also known as *raldh2*; a retinoic acid (RA)-synthesizing enzyme expressed in the epicardium upon heart injury (Fig. 2D) (Kikuchi et al., 2011b; Lepilina et al., 2006)], fibronectin 1a [*fn1a*; an epicardially expressed gene that is required for zebrafish heart regeneration (Wang et al., 2013)] and other key epicardial transcription factors: *tcf21* and *tbx18* (Fig. S1) (Kikuchi et al., 2011a).

The epicardium serves as a cell source and signaling hub for heart regeneration (Cao and Poss, 2018). Paracrine signals from the epicardium that support CM proliferation include the growth factor neuregulin 1 (Nrg1) and follistatin-like 1 (Fstl1) (de Bakker et al., 2021; Gemberling et al., 2015; Wei et al., 2015). We analyzed the genomic regions that included *nrg1*, *fstl1a* or *fstl1b* to help understand their regulation. Our analysis indicates the presence of at least two distinct transcripts of *nrg1* (*nrg1-202* and *nrg1-205*). Two promoters and three putative enhancers are identified for *nrg1* (Fig. S1E). Further motif analysis of these five regions indicates the presence of numerous binding sites for TF activator protein 1 (AP-1) subunits, retinoid X receptors (RXRA and RXRG) and retinoic acid receptors (RARA, RARB and RARG) (Fig. S2 and Table S3). This result suggests that the AP-1 complex and RA signaling may regulate *nrg1* expression during heart regeneration. For the follistatin-like factors, we identified increased transcript levels and several ATAC-seq peaks with increased accessibility for both genes during regeneration (Fig. S3A,B). *In situ* hybridization indicated injury-induced expression in presumed epicardial cells for each gene (Fig. S3A,B).

Motif and pathway enrichment analysis of regions with context-specific accessibility changes

Recurrent consensus motifs that gain active enhancer marks are likely to contain binding sites for transcription factors (TFs). To identify candidate transcriptional regulators active in epicardial cells during heart regeneration, we assayed for enriched nucleotide motifs within regions with differential accessibility at 3 dpa (versus Ctrl) using HOMER (Heinz et al., 2010). Among the top hits of regions with increased accessibility are binding motifs of the AP-1 complex subunits, such as Atf3 (activating transcription factor 3), JunB and Fos (Fig. 2E), which are present in about half of the analyzed regions. These subunits are highly expressed in the epicardium (Table S4), and *in situ* hybridization results indicated expression of *junba* in presumed epicardial cells both before and after heart injury (Fig. 2F). The AP-1 complex was recently implicated in the control of CM gene expression during zebrafish heart regeneration (Beisaw et al., 2020). In agreement with our finding, a recent preprint also reported the increased presence of the AP-1 complex subunit binding motifs in ATAC-seq peaks preferentially accessible in the injured epicardium (Weinberger et al., 2021 preprint). However, AP-1 motifs are common within regulatory sequences (Umer et al., 2019 preprint), and thus a requirement for these motifs might not reflect specificity for regeneration-related gene expression. Other enriched motifs highlight pathways and TFs known to regulate epicardium development and/or regeneration are Tcf21 (Hu et al., 2020), Runx1 (runt-related transcription factor 1) (Koth et al., 2020), the Hippo/Yap pathway (TEA domain family members, TEADs) (Xiao et al., 2018), C/EBPb (CCAAT/enhancer-binding protein b) (Huang et al., 2012), the TGFβ pathway (Smad2/3/4) (Chablais and Jazwinska, 2012) and the Hedgehog pathway (GLI family zinc finger 2, Gli2) (Choi et al., 2013; Sugimoto et al., 2017; Wang et al., 2015). Additional implicated TFs that have not been connected to epicardial functions include NFATC1 (nuclear factor of activated T cells 1), Nrf2 (nuclear factor-E2-related factor 2), Stat3, FoxO1 (Forkhead box O1), FoxO3, FoxO6 and ZBTB7A (zinc finger and BTB domain containing 7A) (Fig. 2E). Interestingly, the top hits of regions with decreased accessibility are binding motifs of Tcf21 and WT1, which are signature TFs of the epicardium. This may suggest a transition in cell state, which may warrant further investigation. Other enriched top hits include motifs belonging to Gata6 (Kolander et al., 2014), ERG (ETS

Development (2022) 149, dev200133. doi:10.1242/dev.200133

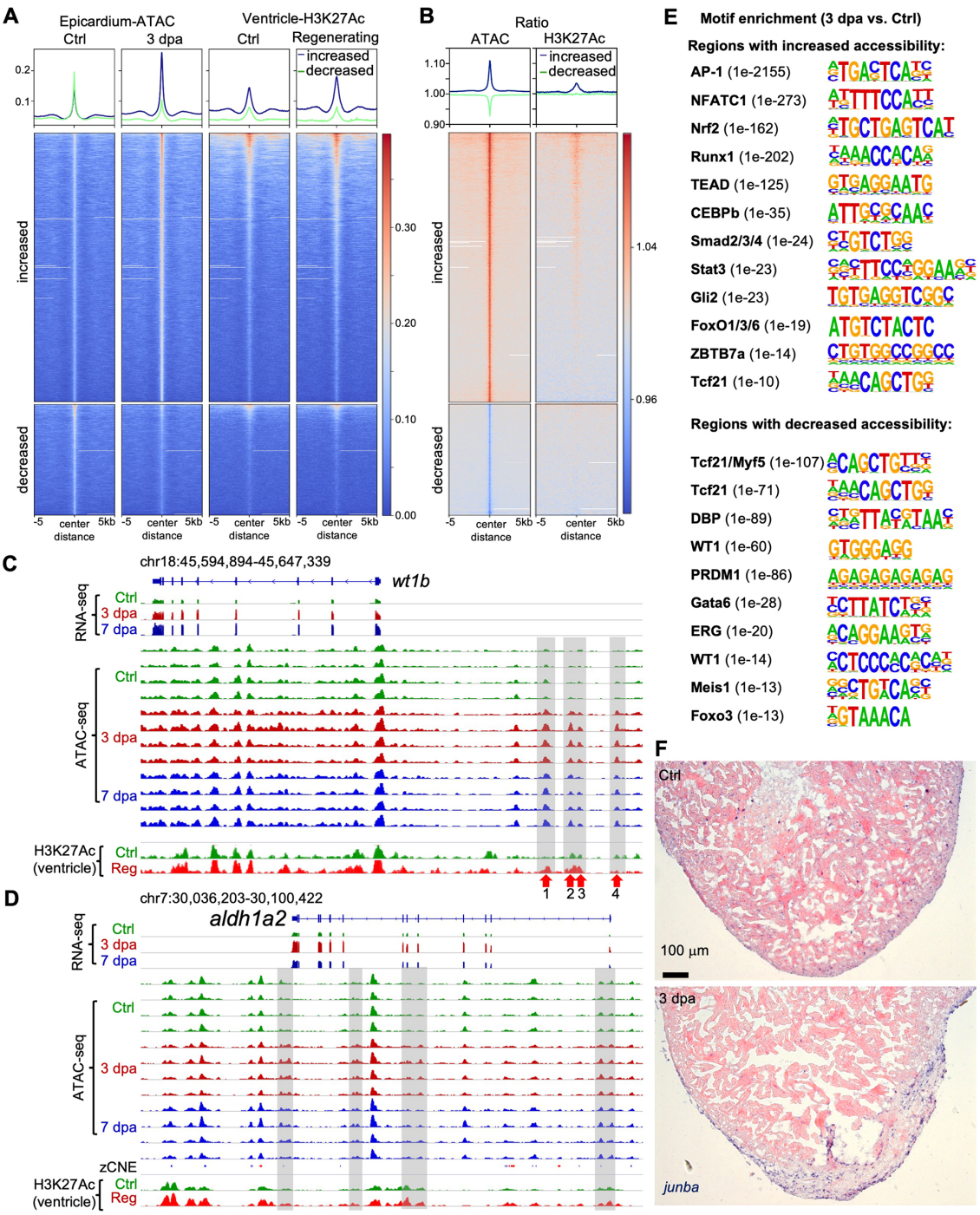

Fig. 2. Chromatin accessibility indicates regulatory programs of epicardium during heart regeneration. (A) Heat map with signals of ATAC-seq and ChIP-seq within ±5 kb of the peak centers. The blue and green lines at the top represent mean read densities of the corresponding ATAC-seq peaks with increased and decreased chromatin accessibility (3 dpa versus Ctrl), respectively. (B) Heat map indicates ratios of the signals shown in A. 3 dpa/Ctrl for ATAC-seq (left) and regenerating/Ctrl for ChIP-seq (right). (C,D) Browser tracks of the genomic region containing the gene *wt1b* or *aldh1a2* showing the transcripts and chromatin accessibility profiles in the epicardium across replicates from Ctrl, 3 dpa and 7 dpa samples. The whole-ventricle H3K27Ac profile of the uninjured (Ctrl) and regenerating (Reg) hearts is shown at the bottom. Gray boxes indicate ATAC-seq peaks with increased accessibility during regeneration. (E) Enriched motifs in the open chromatin regions with increased (top) or decreased (bottom) accessibility at 3 dpa. *P*-value for each enriched TF is shown in the bracket. (F) *In situ* hybridization results show *junba* expression in presumed epicardial cells at 3 dpa and in the uninjured heart. Scale bar: 100 µm.

Transcription Factor ERG), Meis1 (Crespillo et al., 2021; Huang et al., 2012) and Foxo3 (Fig. 2E).

For an overview of biological functions of genes linked to dynamic chromatin regions at 3 dpa, we performed Gene Ontology (GO) enrichment analysis. Compared with epicardial cell samples from uninjured hearts, we found several enriched pathways, including the TGFβ signaling pathway and FoxO signaling pathway, that match the motif analysis results (Table S5). The FoxO pathway regulates many cellular physiological processes, such as apoptosis, cell cycle, metabolism and oxidative stress resistance, by acting downstream of growth factors, insulin, glucose, TGFβ and other stimulators (Lu and Huang, 2011; Nakae et al., 2001; Wang et al., 2014). Other enriched

Development (2022) 149, dev200133. doi:10.1242/dev.200133

pathways include cellular senescence and adherens junctions. It was recently reported that p53 induces senescence in mouse epicardial cells upon heart injury, and induced cellular senescence promotes neonatal heart regeneration (Feng et al., 2019; Sarig et al., 2019). The abovementioned transcription factor Nrf2 and Stat3 are key regulators of cellular senescence (Yan et al., 2021). The enriched processes of blood vessel development and angiogenesis are consistent with the role of the epicardium in supporting revascularization during regeneration (Marin-Juez et al., 2019; Wang et al., 2015) (Fig. S4 and Table S5). Biological processes such as mesenchymal cell development and differentiation, and stem cell development and differentiation implicate the progenitor feature of the epicardial cells. Other enriched processes include heart morphogenesis, apoptotic signaling pathway, cell migration involved in heart development and, unexpectedly, axon development-related processes (Table S5). Enriched molecular functions further emphasize ligand-receptor activities, extracellular matrix binding and SMAD binding (Table S5).

Direct tests of candidate regulatory elements for enhancer activity during regeneration

To prioritize a list of candidates for functional validation of enhancer activity, we first examined the top 20 distal regions with the highest fold increases in accessibility during heart regeneration (Fig. 3A). These peaks were assigned to nearest genes, which included *fn1a* (Wang et al., 2013), neural cell adhesion molecule 1a [*ncam1a*; a gene involved in axon development (Siles et al., 2018);

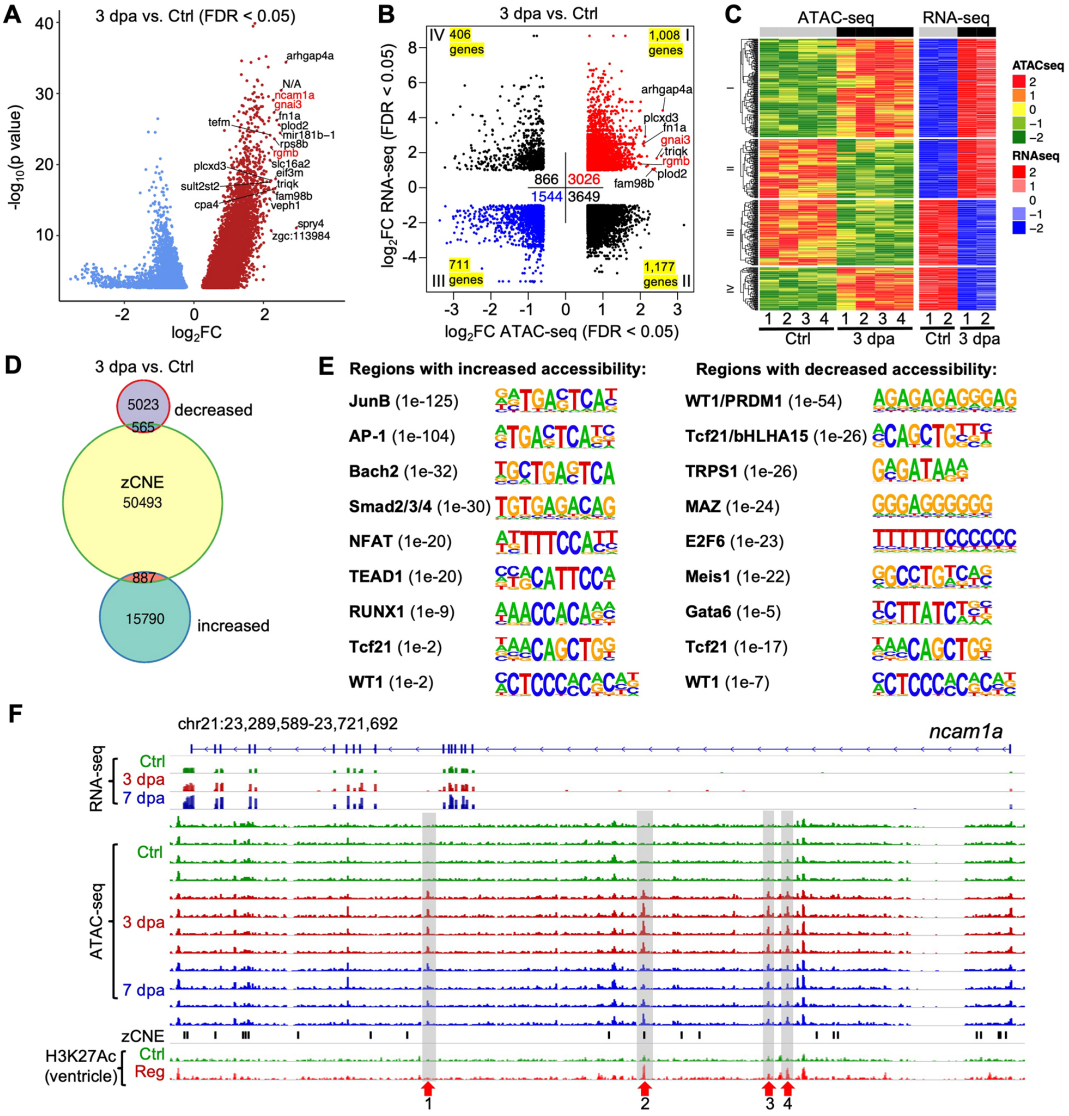

Fig. 3. Candidate regulatory elements for enhancer activity during heart regeneration. (A) Volcano plot of differential ATAC-seq peaks in 3 dpa versus uninjured (Ctrl) samples. The top 20 upregulated peaks with the highest fold changes are marked with the annotated genes. *ncam1a*, *gnai3* and *rgmb* are in red. N/A, no gene is annotated to the peak. (B) Dot plot of differential ATAC-seq peaks linked to nearby differential transcripts in 3 dpa versus uninjured (Ctrl) samples. Each dot indicates an individual ATAC-seq peak and is counted into the total peak numbers of each quadrant. The number of unique genes in each quadrant is indicated in each corner. The most differential peaks of a few genes are marked with *gnai3* and *rgmb* in red. (C) Heat map of differential transcripts in 3 dpa versus uninjured (Ctrl) linked to nearby differentially accessible chromatin regions. (D) Venn diagram comparison of differentially regulated ATAC-seq peaks in 3 dpa versus uninjured compared with the zCNE list. (E) Enriched motifs in the conserved open chromatin regions with increased (left) or decreased (right) accessibility at 3 dpa. *P*-value for each enriched TF is shown in the bracket. (F) Browser tracks of the genomic region near gene *ncam1a* showing the transcripts and chromatin accessibility profiles in the epicardium. The whole-ventricle H3K27Ac profile of the uninjured (Ctrl) and regenerating (Reg) heart is shown at the bottom. zCNE sites are depicted as short black bars. Gray boxes, red arrows and numbers indicate candidate TREEs.

Development (2022) 149, dev200133. doi:10.1242/dev.200133

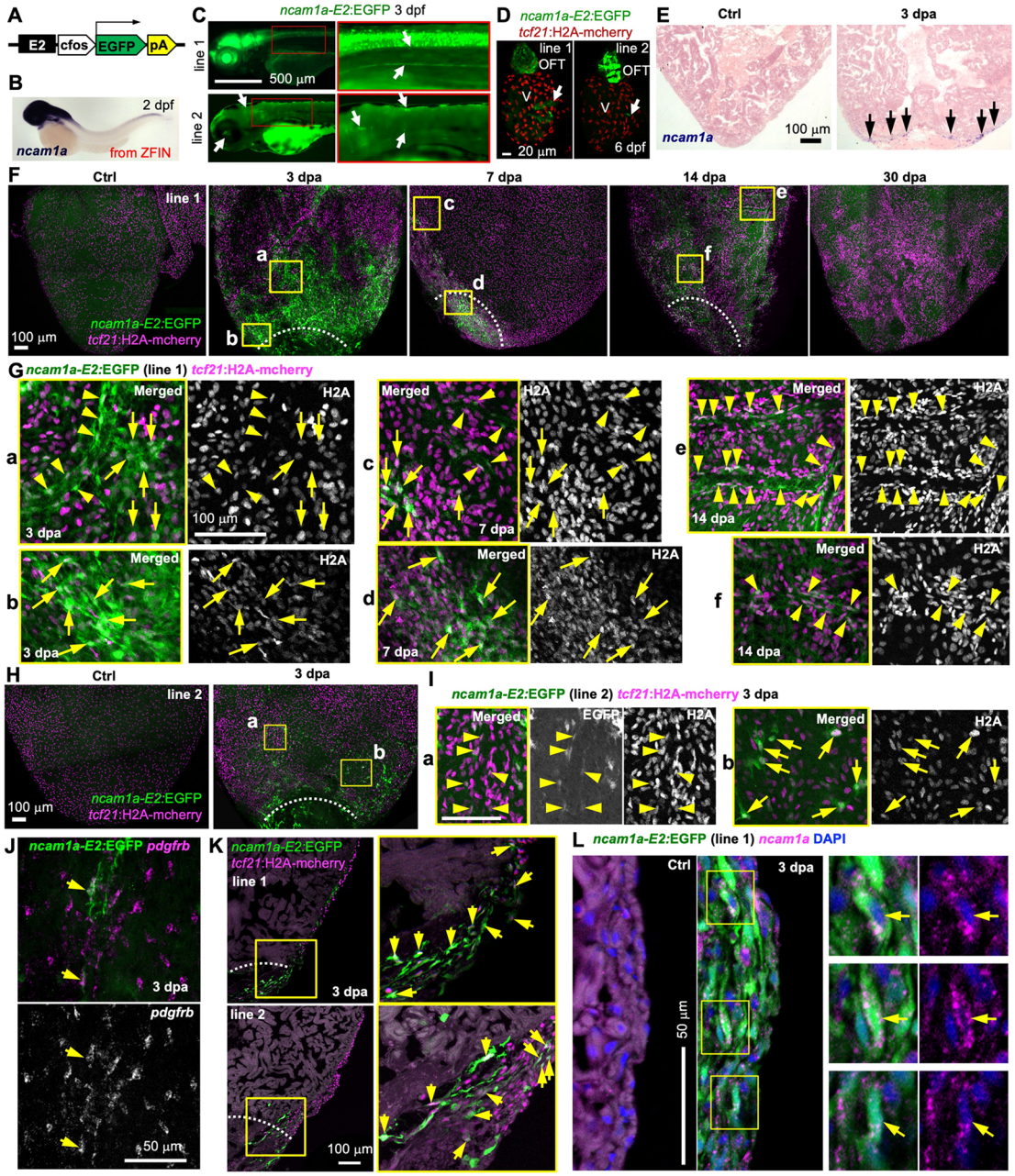

Fig. 4. *ncam1a-E2* directs injury-induced epicardial gene expression. (A) The *ncam1a-E2:EGFP* reporter construct. (B) Whole-mount *in situ* hybridization showing *ncam1a* expression in a 2 dpf embryo. Adapted, with permission, from ZFIN (Ruzicka et al., 2019; Thisse and Thisse, 2004; Thisse et al., 2008). (C) Larval expression of *ncam1a-E2:EGFP* lines at 3 dpf. Higher magnification views of the outlined regions are shown on the right. Scale bar: 500 µm. Arrows indicate representative EGFP signals. (D) Whole-mount images of 6 dpf hearts showing EGFP expression in the outflow tract (OFT) and the atrioventricular valves (arrows). *tcf21*:H2A-mCherry (red) labels the epicardial cells. V, ventricle. Arrows indicate EGFP signals in the atrioventricular valve. Scale bar: 20 µm. (E) *In situ* hybridization results showing *ncam1a* expression in presumed epicardial cells around the injury site at 3 dpa (arrows). Arrows indicate representative *in situ* signals. Scale bar: 100 µm. (F) Whole-mount images (maximum projections of *z*-stacks) of the ventricular surface showing expressions of *ncam1a-E2:EGFP* line 1 (green) in uninjured (Ctrl) and 3, 7, 14 and 30 dpa samples. *tcf21*:H2A-mCherry (magenta) labels the epicardial cells. White dashed lines indicate the injury sites. The regions outlined in yellow are enlarged in G. Scale bar: 100 µm. (G) Single optical slice of confocal images of the outlined regions in F. Arrows and arrowheads indicate representative cells that express both EGFP (green) and *tcf21*:H2A-mCherry (magenta). Arrowheads in a,c,e,f also indicate possible *tcf21*$^{+}$ perivascular cells. Scale bar: 100 µm. (H) Whole-mount images (maximum projections) of the ventricular surface showing expression of *ncam1a-E2:EGFP* line 2 (green) in uninjured (Ctrl) and 3 dpa samples. Magnified views of the outlined region are shown in I. (I) Single optical section of confocal images of the outlined regions in H. Single-channel images are shown in grayscale. Arrows and arrowheads (presumed perivascular) indicate representative double-positive cells. Scale bar: 100 µm. (J) HCR staining result of *pdgfrb* (magenta) on a whole-mounted heart carrying the *ncam1a-E2:EGFP* reporter (line 2, green, anti-EGFP antibody staining). Single-channel image shows staining signals of *pdgfrb*. Arrows indicate EGFP^{+}*pdgfrb*$^{+}$ cells. Scale bar: 50 µm. (K) Section images demonstrating expression of *ncam1a-E2:EGFP* (green) in *tcf21*:H2A-mCherry^{+} (magenta) cells. Magnified views of the outlined regions are shown on the right. White dashed lines indicate the injury sites. Scale bar: 100 µm. Arrows indicate representative double-positive cells. (L) HCR staining of *ncam1a* (magenta dots) on ventricular sections (ctrl, 3 dpa) showing *ncam1a-E1:EGFP* expression (line 1, green) in *ncam1a*$^{+}$ cells. The outlined regions are enlarged on the right. Arrows indicate EGFP^{+}*ncam1a*$^{+}$ cells. No definitive epicardial expression of *ncam1a* was observed in the Ctrl samples. Some nonspecific background staining is evident in the muscle. Scale bar: 50 µm.

Development (2022) 149, dev200133. doi:10.1242/dev.200133

listed by the enrichment annotation results in Fig. S4 and Table S5], repulsive guidance molecule BMP co-receptor b [*rgmb*; encoding a TGFβ superfamily signaling component that participates in neuronal development (Liu et al., 2016; Samad et al., 2005) (Table S5)] and guanine nucleotide binding protein, alpha inhibiting activity polypeptide 3 (*gnai3*; encoding a G protein). We next combined the bulk RNA-seq and ATAC-seq datasets, and identified 3026 ATAC-peaks with their related 1008 genes and RNA levels, with both features increased at 3 dpa (Fig. 3B, red dots; Fig. 3C; Table S6). Eight of the top 20 distal regions with increased accessibility during regeneration are on the list. These eight regions are assigned to genes *fn1a*, *rgmb*, *gnai3*, Rho GTPase activating protein 4a (*arhgap4a*), procollagen-lysine 2-oxoglutarate 5-dioxygenase (*plod2*), phosphatidylinositol-specific phospholipase C X domain containing 3 (*plcxd3*), triple QxxK/R motif containing (*triqk*) or family with sequence similarity 98 member B (*fam98b*) (Fig. 3B, Figs S1 and S3). Last, we looked for conserved regions by comparing our dataset with the published zebrafish Conserved Non-genic Elements (zCNEs) database, which contains conserved regions from fish to human (Hiller et al., 2013). We identified 887 ATAC-seq peaks that contain conserved regions and gain accessibility at 3 dpa (Fig. 3D and Table S7), including a top differential peak assigned to *ncam1a* (Fig. 3F, enhancer 2 or E2). 565 decreased ATAC-seq peaks also contain conserved regions. Motif analysis of these differentially regulated regions yielded a comparable result (Fig. 3E) to that of all differential peaks (Fig. 2E), with the AP-1 motifs being the most positive regulators, and Tcf21 and WT1 motifs being the most negative regulators. This result may suggest a conserved epicardial regeneration program. As an example of conserved ATAC-seq peaks, Fig. 3F shows four emerging ATAC-seq regions residing in intronic regions of *ncam1a*, which increase accessibility at both 3 and 7 dpa. *ncam1a-E2* (+181 kb), which is among the top 20 regions (Fig. 3A), contains conserved sequences and displays strong enrichment with histone H3K27Ac marks in samples of whole regenerating ventricles. *ncam1a-E4* (+110 kb) also has a significantly enriched histone H3H27Ac signature. To select candidate enhancers for functional evaluations, we performed *in situ* hybridization for *ncam1a*, *rgmb*, *gnai3*, *plod2*, *triqk*, *plcxd3* and *arhgap4a*, observing induced transcript expression for all genes apart from *arhgap4a* in presumed epicardial cells upon injury (Fig. S3 and the following text). Regions of the first three genes received the highest priority for functional tests in transgenic lines, given that they have not yet been implicated in epicardial biology.

Distinct *ncam1a*-linked TREEs direct different domains of epicardial gene expression during heart regeneration

The human homolog *NCAM1* encodes a cell adhesion protein of the immunoglobulin superfamily that regulates cell-cell and cell-matrix interactions during development and differentiation processes (Duncan et al., 2021; Siles et al., 2018). We searched for *ncam1a* in the Zebrafish Regeneration Database that includes published transcriptome datasets of heart, fin or spinal cord regeneration (http://zfregeneration.org) (Nieto-Arellano and Sanchez-Iranzo, 2019), finding that *ncam1a* RNA levels increased during regeneration of all three tissues (Fig. S5). To test the efficacy of these candidate enhancers, we subcloned each regulatory region upstream of a *c-fos* minimal promoter and *EGFP* cassette (Fig. 4A). Without a regulatory sequence, this cassette has minimal expression in embryos and adult hearts, even after cardiac injury (Goldman et al., 2017). Multiple stable lines were established. We identified two stable lines for *ncam1a-E2:EGFP*. In 3 dpf larvae, line 1 directs strong EGFP expression in the eye, brain, spinal cord and notochord, resembling *ncam1a* expression in the embryo [Fig. 4B (adapted, with permission, from ZFIN) (Ruzicka et al., 2019; Thisse and Thisse, 2004; Thisse et al., 2008), Fig. 4C]. Line 2 has dimmer expression, but EGFP signals are still visible in these tissues (Fig. 4C). In addition, whole-mount images of dissected 6 dpf (days post-fertilization) hearts indicate EGFP expression primarily in the outflow tract and atrioventricular valves, but not in *tcf21*$^+$ epicardial cells (Fig. 4D). After resection of the adult ventricle, we observed *ncam1a* expression in the ventricular surface, which is enriched around the injury site at 3 dpa, suggesting an epicardial expression pattern (Fig. 4E). Similarly, images of both *ncam1a-E2:EGFP* lines demonstrated injury-induced EGFP expression around the wound at 3 and 7 dpa in *tcf21*:H2A-mCherry$^+$ cells (Fig. 4F-K). In addition, we observed mCherry$^+$EGFP$^+$ cells aligned in parallel and these EGFP$^+$ cells expressed the mural cell marker *pdgfrb* (Ando et al., 2021) (Fig. 4G, arrowheads; Fig. 4J, arrows), suggesting *ncam1a-E2* activity in *tcf21*$^+$ perivascular cells. By 14 dpa, EGFP expression is much weaker but broadly distributed across the entire ventricular surface and primarily in the perivascular cells (Fig. 4F,Ge,f). EGFP was almost undetectable at 30 dpa (Fig. 4F). Although line 2 has lower embryonic expression than line 1, its adult heart expression pattern is consistent with line 1 (Fig. 4H,I,K; data not shown). To test whether *ncam1a-E2* is active specifically in *ncam1a*-expressing cells, we performed hybridization chain reaction (HCR) staining (Choi et al., 2018) of heart sections carrying the enhancer reporters. As shown in Fig. 4L, *ncam1a-E2:EGFP* is expressed in *ncam1a*$^+$ cells upon injury confirming its specific activity linked to the target gene. We also noticed *ncam1a* expression in EGFP$^-$ cells, suggesting that *ncam1a-E2* only contributes partially to the injury-induced *ncam1a* expression in the heart. No definitive *ncam1a* expression was detected in the uninjured ventricles.

We next characterized *ncam1a-E4*. Three *ncam1a-E4:EGFP* lines displayed very weak whole-body larval EGFP expression without clear tissue specificity (Fig. 5A,B). With an anti-EGFP antibody staining in adult hearts, we consistently observed a small population of EGFP$^+$; *tcf21*:H2A-mCherry$^+$ cells on the ventricular surface after injury (Fig. 5C). Enhancers may reside upstream or downstream of the TSS of the regulated gene and may function together as a cluster to exert additive and synergistic actions (Choi et al., 2021; Hnisz et al., 2013). We asked whether inserting multiple enhancers in series would enhance the activity, by placing a second *E4* element after the poly-A signal of the *ncam1a-E4:EGFP* construct (Fig. 5D). One stable line was identified (*ncam1a-E4E4:EGFP*) with expression in eye, tail and heart muscles but not larval *tcf21*$^+$ epicardial cells (Fig. 5D,E). Prominent cardiac EGFP in the adults was observed only upon heart injury. At 3 dpa, strong EGFP expression in *tcf21*:H2A-mCherry$^+$ cells was located at the injury site, whereas slightly weaker expression was also observed in the entire epicardium distal to the injury site (Fig. 5F,H), distinguishing its activity from the *ncam1a-E2:EGFP* lines. EGFP expression is reduced after 3 dpa, restricted to the injury site at 7 dpa, and undetectable at 30 dpa (Fig. 5F,G). Unlike *ncam1a-E2*, no definitive perivascular cell expression was observed for either *ncam1a-E4E4:EGFP* or *ncam1a-E4:EGFP* lines. HCR staining further confirmed *ncam1a-E4E4:EGFP* expression in *ncam1a*$^+$ cells both in the wound region and the distal ventricular regions (Fig. 5I,J). Following the same strategy of stacking enhancers, we asked whether combining two *ncam1a-E2* sequences would enhance its activity (Fig. S6A). Compared with *ncam1a-E2:EGFP*, *ncam1a-E2E2:EGFP* lines had relatively similar EGFP expression in the embryos (Fig. S6B,C). These *ncam1a-E2E2:EGFP* lines demonstrated apparently identical expression

Development (2022) 149, dev200133. doi:10.1242/dev.200133

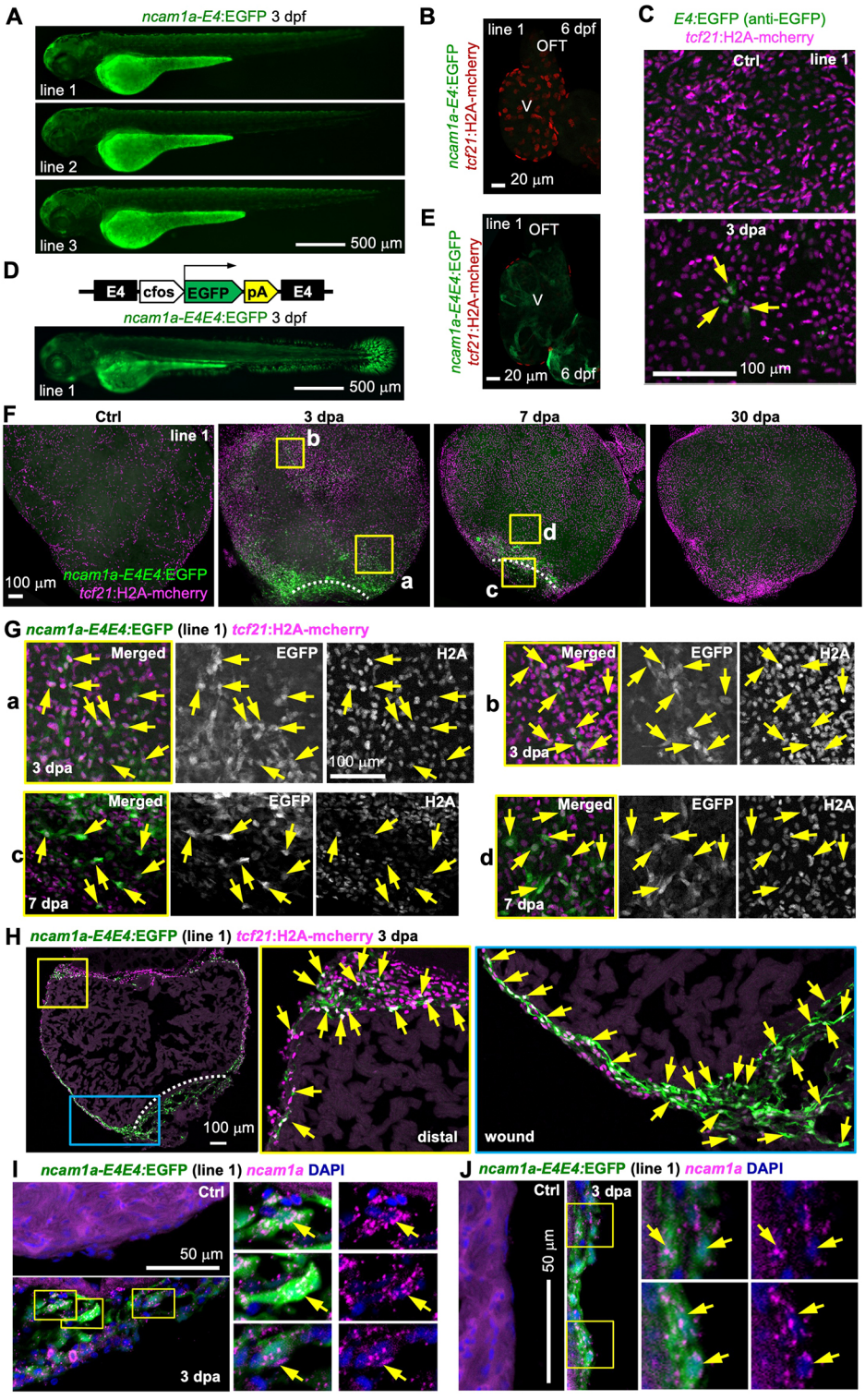

Fig. 5. *ncam1a-E4* directs injury-induced epicardial gene expression. (A) Larval expression of *ncam1a-E4:EGFP* lines. Scale bar: 500 µm. (B) Whole-mount image of a 6 dpf heart with *tcf21*:H2A-mCherry (red) labeling the epicardial cells. No EGFP expression was observed. V, ventricle. Scale bar: 20 µm. (C) Whole-mount images (maximum projections) of the ventricular surface showing expression of a *ncam1a-E4:EGFP* line in uninjured (Ctrl) and 3 dpa samples. Anti-EGFP antibody staining was used to detect the EGFP expression. Scale bar: 100 µm. (D) Top: the *ncam1a-E4E4:EGFP* reporter construct. Bottom: larval expression of *ncam1a-E4E4:EGFP* reporter line. Scale bar: 500 µm. (E) Optical section image of a 6 dpf heart (whole-mounted) showing EGFP expression in the muscle. *tcf21*:H2A-mCherry (red) labels the epicardial cells. V, ventricle. Scale bar: 20 µm. (F) Whole-mount images (maximum projections) of the ventricular surface showing expressions of *ncam1a-E4E4:EGFP* line 1 (green) in uninjured (Ctrl) and 3, 7 and 30 dpa samples. *tcf21*:H2A-mCherry (magenta) labels the epicardial cells. White dashed lines indicate the injury sites. The outlined regions are enlarged in G. Scale bar: 100 µm. (G) Single optical section of confocal images from the regions outlined in F. Single-channel images are shown in grayscale. Arrows indicate representative GFP$^+$mCherry$^+$ cells. Scale bar: 100 µm. (H) Section images demonstrating expression of *ncam1a-E4E4:EGFP* (green) in *tcf21*:H2A-mCherry$^+$ (magenta) cells. Magnified views of the outlined regions are shown on the right (distal and wound regions). White dashed lines indicate the injury sites. Arrows indicate representative double-positive cells. Scale bar: 100 µm. (I,J) HCR staining of *ncam1a* (magenta dots) on ventricular sections (ctrl, 3 dpa) showing *ncam1a-E4E4:EGFP* expression (green) in *ncam1a*$^+$ cells both in the wound (I) and distal (J) regions. The outlined regions are enlarged on the right. Arrows indicated EGFP$^+$*ncam1a*$^+$ cells. Scale bars: 50 µm.

patterns and the same trend of expression levels as the *ncam1a-E2:EGFP* reporters (peaked at 3 dpa, decreased through 30 dpa; Fig. S6D-H). Although larval expression was variable between lines of each enhancer construct, adult epicardial expression was remarkably consistent across lines. These results suggest that *ncam1a-E2* and *ncam1a-E4* are epicardial TREEs that regulate *ncam1a* expression during heart regeneration. Interestingly, their distinct expression dynamics indicate that individual enhancers may combine to generate an overall expression domain. This is comparable with the overlapping but distinct activities of multiple developmental enhancers linked to one gene (Dickel et al., 2018; Dunipace et al., 2019; Osterwalder et al., 2018), a regulatory strategy that ostensibly applies to regeneration contexts.

A *rgmb*-linked TREE directs injury-induced epicardial gene expression

Rgmb, a TGFβ superfamily signaling component, has been reported to bind to BMP2 or BMP4 as a co-receptor, to pattern

Development (2022) 149, dev200133. doi:10.1242/dev.200133

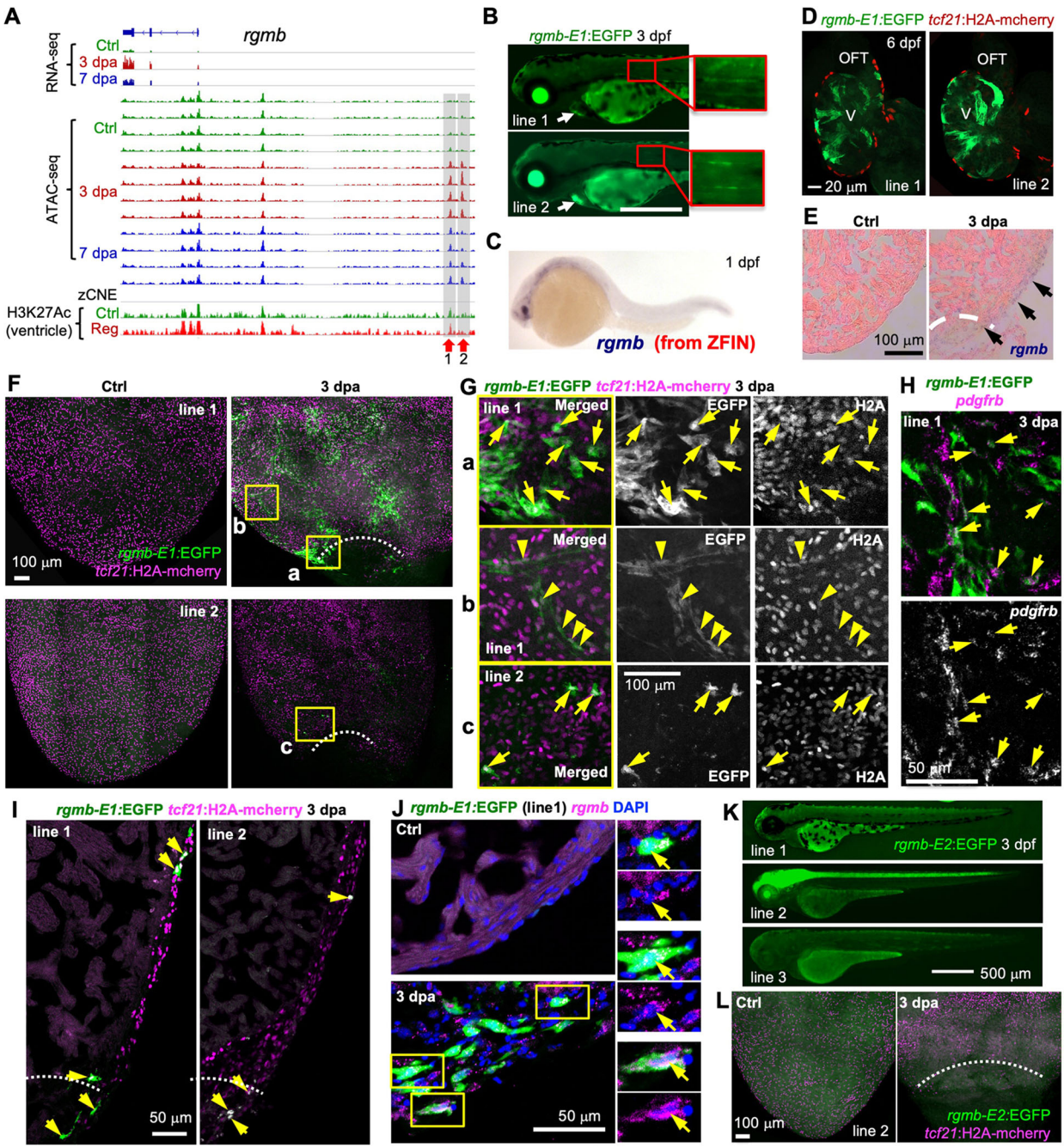

Fig. 6. A *rgmb*-linked TREE directs injury-induced epicardial gene expression. (A) Browser tracks of the genomic region near gene *rgmb* showing the transcripts and chromatin accessibility profiles in the epicardium. The whole-ventricle H3K27Ac profile of the uninjured (Ctrl) and regenerating (Reg) heart is shown at the bottom. Gray boxes, red arrows and numbers indicate candidate TREEs. (B) Larval expression of *rgmb-E1:EGFP* lines at 3 dpf. Arrows indicate the heart. Scale bar: 500 µm. (C) Whole-mount *in situ* hybridization showing *rgmb* expression in a 1 dpf embryo. Adapted, with permission, from ZFIN (Ruzicka et al., 2019; Thisse and Thisse, 2004; Thisse et al., 2008). (D) Optical section images of 6 dpf hearts (whole-mounted) showing EGFP expression in the muscle. *tcf21*:H2A-mCherry (red) labels the epicardial cells. V, ventricle. Scale bar: 20 µm. (E) *In situ* hybridization results showing injury-induced *rgmb* expression on the ventricular surface (arrows) at 3 dpa. Dashed line indicates the injury site. (F) Whole-mount images (maximum projections) of the ventricular surface showing expression of the *rgmb-E1:EGFP* reporter lines (green, anti-EGFP antibody staining) in uninjured (Ctrl) and 3 dpa samples. *tcf21*:H2A-mCherry (magenta) labels the epicardial cells. White dashed lines indicate the injury sites. The outlined regions are enlarged in G. Scale bar: 100 µm. (G) Single optical sections of confocal images of the outlined regions in F. Single-channel images are shown in grayscale. Arrows and arrowheads indicate representative EGFP^{+}mCherry^{+} cells. Arrowheads in b indicate presumed perivascular cells. Scale bar: 100 µm. (H) HCR staining result of *pdgfrb* (magenta) on a whole-mount heart carrying the *rgmb-E1:EGFP* reporter (line 1, green, anti-EGFP antibody staining). Single-channel image shows staining signals of *pdgfrb*. Arrows indicate EGFP^{+}*pdgfrb*$^{+}$ cells. Scale bar: 50 µm. (I) Section images demonstrating expression of *rgmb-E1:EGFP* (green, anti-EGFP antibody staining) in *tcf21*:H2A-mCherry^{+} (magenta) cells. Arrows indicate representative double-positive cells. Scale bar: 50 µm. (J) HCR staining of *rgmb* (magenta dots) on ventricular sections (ctrl, 3 dpa) showing *rgmb-E1:EGFP* expression (green, anti-EGFP antibody staining) in *rgmb*$^{+}$ cells. The outlined regions are enlarged on the right. Arrows indicate EGFP^{+}*rgmb*$^{+}$ cells. Scale bar: 50 µm. (K) Larval expression of *rgmb-E2:EGFP* lines. Scale bar: 500 µm. (L) Whole-mount images (maximum projections) of the ventricular surface showing no EGFP induction in the 3 dpa sample carrying the *rgmb-E2:EGFP* reporter. *tcf21*:H2A-mCherry (magenta) labels the epicardial cells. White dashed lines indicate the injury site. Scale bar: 100 µm.

Development (2022) 149, dev200133. doi:10.1242/dev.200133

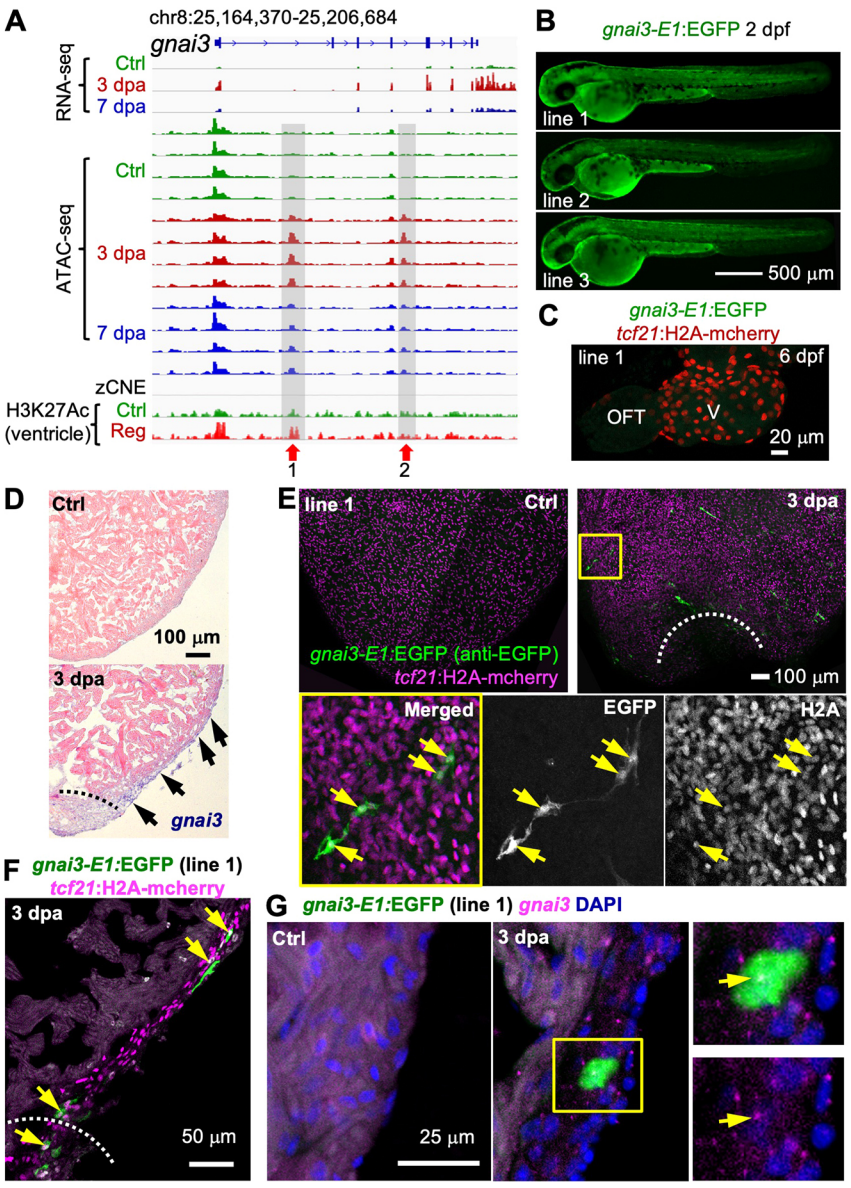

Fig. 7. A *gnai3*-linked TREE directs injury-induced epicardial gene expression. (A) Browser tracks of the genomic region near *gnai3* showing the transcripts and chromatin accessibility profiles in the epicardium, the zCNE sites and the whole-ventricle H3K27Ac profile. Gray boxes, red arrows and numbers indicate candidate TREEs. (B) Larval expression of three *gnai3-E1:EGFP* reporter lines. Scale bar: 500 µm. (C) Whole-mount image of a 6 dpf heart showing no GFP expression. *tcf21*:H2A-mCherry (red) labels the epicardial cells. V, ventricle. Scale bar: 20 µm. (D) *In situ* hybridization results showing *gnai3* expression in presumed epicardial cells (arrows) at 3 dpa. Dashed line indicates the injury site. Scale bar: 100 µm. (E) Whole-mount images (maximum projections) of the ventricular surface showing *gnai3-E1:EGFP* expression in *tcf21*:H2A-mCherry^{+} cells. An enlarged view of the outlined region is displayed at the bottom with single-channel image shown in grayscale (single optical sections). White dashed line indicates the injury sites. Arrows indicate representative EGFP^{+}mCherry^{+} cells. Scale bar: 100 µm. (F) Section images demonstrating expression of *gnai3-E1:EGFP* (green, anti-EGFP antibody staining) in *tcf21*:H2A-mCherry^{+} (magenta) cells. Arrows indicate representative double-positive cells. Scale bar: 50 µm. (G) HCR staining of *gnai3* (magenta dots) on ventricular sections (ctrl, 3 dpa) showing *gnai3-E1:EGFP* expression (green, anti-EGFP antibody staining) in *gnai3*$^{+}$ cells. The outlined region is enlarged on the right. Arrows indicate an EGFP^{+}*gnai3*$^{+}$ cell. Scale bar: 25 µm.

the developing nervous system or to inhibit renal cyst development (Liu et al., 2016; Samad et al., 2005). Although no function of *rgmb* in heart regeneration has been reported, *bmp2b* overexpression enhances CM proliferation after cardiac injury in zebrafish (Wu et al., 2016). *rgmb* RNA levels increased at 3 dpa [$\log_2$FC=1.74, Padj (adjusted *P*-value)=7.42E-12] and 7 dpa ($\log_2$FC=1.38, Padj=1.92E-06) in our datasets (Table S4). The Zebrafish Regeneration Database recorded increases in *rgmb* RNA levels in heart or spinal cord regeneration, consistent with a pro-regenerative function in different tissues (Fig. S7). Two putative enhancers (*rgmb-E1*, −68 kb; *rgmb-E2*, −71 kb) upstream of the TSS were identified from our analyses, with *rgmb-E1* showing enriched H3K27Ac marks in whole-ventricle samples (Fig. 6A). Multiple stable lines were established for each candidate enhancer. We found that *rgmb-E1* sequences directed strong EGFP expression in F1 embryos, including heart, eye and notochord expression (Fig. 6B), which resembled the published *in situ* hybridization findings (Fig. 6C, adapted, with permission, from ZFIN) (Ruzicka et al., 2019; Thisse and Thisse, 2004; Thisse et al., 2008). Cardiac expression in the 6 dpf larvae was restricted to the myocardium but not the epicardium (Fig. 6D). In adult hearts, injury-induced *rgmb* transcripts were detected on the ventricular surface (Fig. 6E). For the *rgmb-E1* reporter lines, EGFP expression in adult epicardial cells (*tcf21*:H2A-mCherry^{+}) was induced after a heart injury, both locally and distal to the injury site (Fig. 6F-I), including expression in *pdgfrb*$^{+}$ perivascular cells (Fig. 6H), suggesting that *rgmb-E1* is an epicardial TREE. We noticed patchy EGFP expression that was often adjacent to vessels (Fig. 6F-H). This may suggest pro-angiogenic or related functions of *rgmb*. HCR staining confirmed that *rgmb-E1* activity is restricted to *rgmb*$^{+}$ cells (Fig. 6J). However, numerous *rgmb*$^{+}$EGFP^{-} cells were observed in the epicardium, indicating that *rgmb-E1* only contributes partially to the gene activity. By contrast to *rgmb-E1*, three stable lines of *rgmb-E2:EGFP* were identified without consistent EGFP expression in larval or adult hearts (Fig. 6K,L). These results indicate that, whereas *rgmb-E1* is sufficient to direct injury-induced gene expression, *rgmb-E2* on its own is inadequate.

Development (2022) 149, dev200133. doi:10.1242/dev.200133

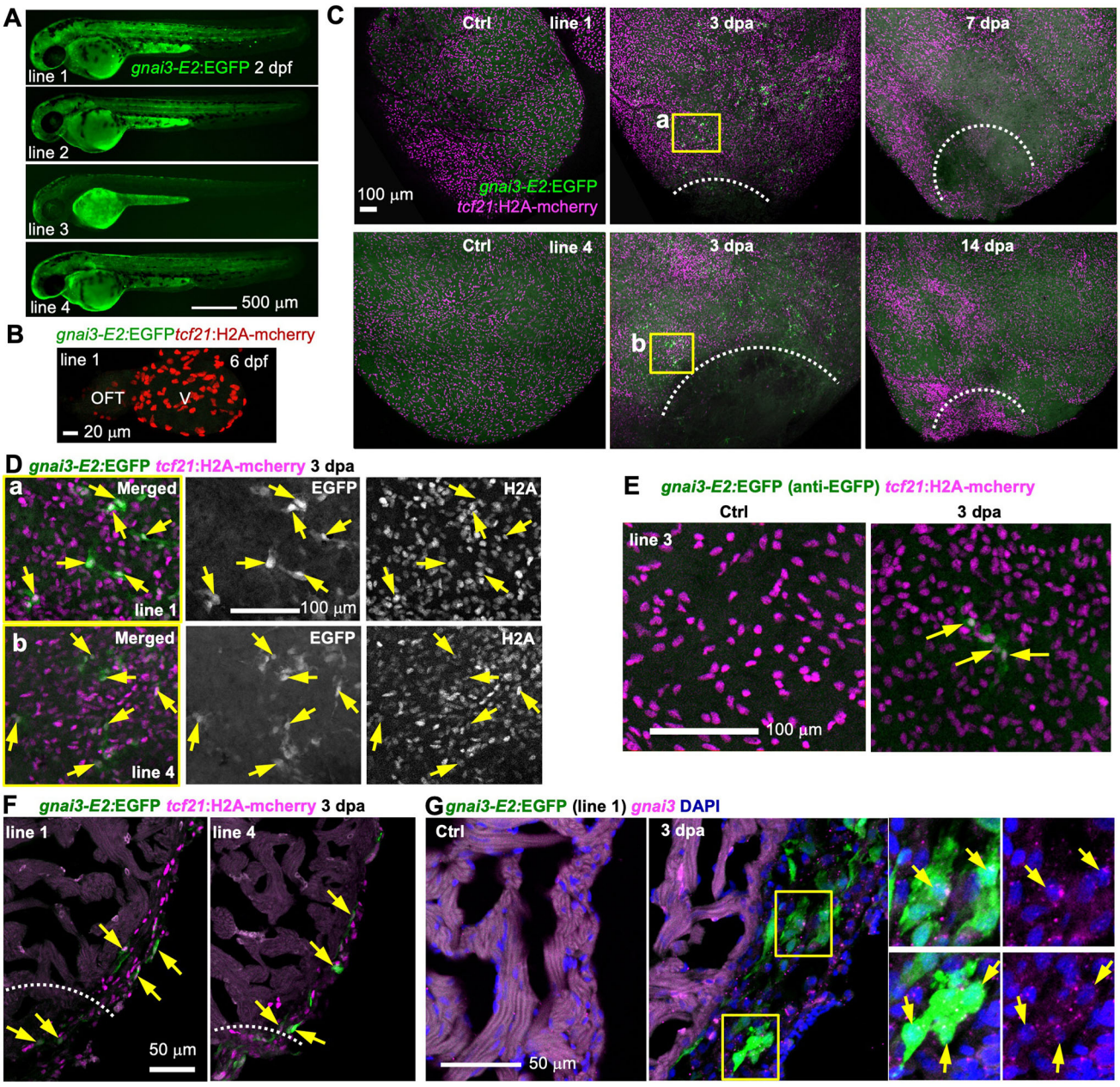

Fig. 8. *gnai3-E2* directs similar injury-induced epicardial gene expression as *gnai3-E1*. (A) Larval expression of four *gnai3-E2:EGFP* reporter lines. Scale bar: 500 µm. (B) Whole-mount image of a 6 dpf heart showing no EGFP expression. *tcf21*:H2A-mCherry (red) labels the epicardial cells. V, ventricle. Scale bar: 20 µm. (C) Whole-mount images (maximum projections) of the ventricular surface showing expression of the *gnai3-E2:EGFP* lines 1 and 4 (green) in uninjured (Ctrl) and 3, 7 and 14 dpa samples. *tcf21*:H2A-mCherry (magenta) labels the epicardial cells. White dashed lines indicate the injury sites. The outlined regions are enlarged in D. Scale bar: 100 µm. (D) Single optical section of confocal images of the outlined regions in C. Single-channel images are shown in grayscale. Arrows indicate representative EGFP$^+$mCherry$^+$ cells. Scale bar: 100 µm. (E) Whole-mount images (maximum projection) showing expression of the *gnai3-E2:EGFP* reporter line 3. A few EGFP$^+$; *tcf21*:H2A-mCherry$^+$ cells were seen upon injury (arrows). Scale bar: 100 µm. (F) Section images demonstrating expression of *gnai3-E2:EGFP* (green, anti-EGFP antibody staining) in *tcf21*:H2A-mCherry$^+$ (magenta) cells. Arrows indicate representative double-positive cells. Scale bar: 50 µm. (G) HCR staining of *gnai3* (magenta dots) on ventricular sections (ctrl, 3 dpa) showing *gnai3-E2:EGFP* expression (green, anti-EGFP antibody staining) in *gnai3*$^+$ cells. The outlined regions are shown on the right. Arrows indicate EGFP$^+$*gnai3*$^+$ cells. Scale bar: 50 µm.

Distinct *gnai3*-linked TREEs direct similar injury-induced epicardial gene expression

Gnai3 is a G protein that binds to G protein-coupled receptors (GPCRs) to regulate various transmembrane signaling pathways (Syrovatkina et al., 2016). The Zebrafish Regeneration Database reports increased RNA levels of *gnai3* during heart, fin and spinal cord regeneration, suggesting functions in multiple regeneration contexts (Fig. S8) (Nieto-Arellano and Sanchez-Iranzo, 2019). In our datasets, *gnai3* RNA was increased at 3 dpa (log_2FC=2.08, Padj=6.43E-11) and 7 dpa (log_2FC=0.85, Padj=0.023) (Table S4). We identified two putative enhancers within intron 1 (*gnai3-E1*, +8.8 kb) and intron 4 (*gnai3-E2*, +21 kb), both of which have H3K27Ac marks in the whole-ventricle profile (Fig. 7A). Three stable lines for *gnai3-E1* and four lines for *gnai3-E2* were established. Each *gnai3-E1:EGFP* line displayed whole-body larval EGFP expression without clear specificity (Fig. 7B). No

Development (2022) 149, dev200133. doi:10.1242/dev.200133

EGFP expression was noticed in larval epicardium by 6 dpf (Fig. 7C). In adult hearts, injury-induced *gnai3* transcripts were detected on the ventricular surface (Fig. 7D). From each of three *gnai3-E1* lines, we consistently observed a small population of EGFP$^+$; *tcf21:*H2A-mCherry$^+$ cells on the ventricular surface after injury (Fig. 7E,F; 3 dpa, based on anti-EGFP antibody staining). HCR staining confirmed EGFP expression in *gnai3*-expressing cells (Fig. 7G).

gnai3-E2:EGFP is expressed in the notochord and regions of skin consistently in several lines, in addition to the weak whole-body expression (Fig. 8A). Similar to *gnai3-E1:EGFP*, no embryonic epicardial expression was seen for *gnai3-E2:EGFP* lines by 6 dpf (Fig. 8B). In adults, images of lines 1 and 4 of *gnai3-E2:EGFP* demonstrated injury-induced expression in epicardial cells at 3 dpa (Fig. 8C,D,F). These expression patterns are diminished by 7 or 14 dpa (Fig. 8C), mimicking the reduced RNA levels of *gnai3* at 7 dpa (Fig. 7A). The injury-induced EGFP expression of line 3 was relatively weak but restricted to *tcf21*$^+$ cells (based on anti-EGFP antibody staining, Fig. 8E). HCR staining confirmed that EGFP expression is restricted to but does not cover all *gnai3*-expressing cells (Fig. 8G). These results suggest that *gnai3-E1* and *gnai3-E2* are epicardial TREEs, and their similar expression dynamics indicate how the expression pattern of one gene during regeneration may receive similar regulatory instructions from two distinct TREEs. Although genes are commonly regulated by multiple enhancers with redundant activities in developmental contexts (reviewed by Kvon et al., 2021), our finding here extends this concept to tissue regeneration.

DISCUSSION

The profiling we present can guide identification of factors that bind and are upstream of candidate and validated regulatory sequences, as well as target genes linked to these sequences, to help elucidate the epicardial injury response during heat regeneration. Huang et al. previously defined epicardial enhancers by analyzing the evolutionarily conserved regions linked to epicardial genes, including *Raldh2* and *Wt1*, and found enhancers that can direct expression both in developing hearts and in response to injury (Huang et al., 2012). By contrast, the epicardial TREEs we identified direct injury-induced but not developmental expression in the epicardium, suggesting they are customized to the epicardial regeneration machinery. Notably, a recent preprint used a similar approach to identify epicardial enhancers, reporting distinct regulatory programs during epicardial development and regeneration (Weinberger et al., 2021 preprint). Enhancers linked to genes *loxa*, *ppfibp1a*, *col12a1a* and *mdka* were found to be sufficient to direct gene expression in the embryonic epicardium, although whether they have enhancer activity during regeneration was not addressed.

In our study, we noticed variations between stable lines employing the same enhancer, likely explained by different genome insertion sites and copy numbers among lines. Establishing and analyzing multiple lines for each candidate enhancer is crucial to define the activity patterns with this transgenic strategy. We found that multiple TREEs linked to a regeneration-regulated gene can possess either matching (*gnai3-E1* and *gnai3-E2*) or partially overlapping/complementary (*ncam1a-E2* and *ncam1a-E4*) regulatory controls, suggesting additive, redundant or synergetic effects of enhancers during regeneration. In this regard, deleting one of the enhancers for each gene may not fully abolish the injury-induced gene expression, which could explain why deletions of single TREEs typically can cause minor or no effect on gene expression (Thompson et al., 2020).

We expect that the epicardial TREEs validated here, as well as putative TREEs implicated by the profiles, can be employed to generate transgenic lines that enable injury-induced expression of gene cassettes, for example, to direct targeted expression of candidate pro-regenerative factors (Kang et al., 2016).

MATERIALS AND METHODS

Zebrafish maintenance and procedures

Adult zebrafish of the Ekkwill and Ekkwill/AB strains were maintained as described previously (Poss et al., 2002; Wang et al., 2011). Briefly, the water temperature was maintained at 28°C, and fish were kept on a 14/10 light/dark cycle at a density of 5-10 fish per liter. Animals of both sexes were used for adult (9-week-old to 12-month-old) experiments. Heart resection injury was carried out as described previously (Poss et al., 2002). No animal was excluded from analyses unless they died after the injury. Published transgenic lines used in this study were *Tg(tcf21:H2A-mCherry)*^{pd252} (Cao et al., 2017) and *Tg(tcf21:nucEGFP)*^{pd41} (Kikuchi et al., 2011a). All transgenic strains were analyzed as hemizygotes. Animal procedures were approved by Animal Care and Use Committees at Duke University and Weill Cornell Medical College.

Generation of transgenic reporters

Putative enhancer regions were amplified from genomic DNA using primers listed in Table S8 and inserted upstream of the 95 bp minimal mouse *c-fos* promoter directing EGFP (Fivaz et al., 2000). The entire *enhancer-fos-EGFP-SV40 poly A* cassette is flanked by two I-Sce meganuclease restriction sites that facilitate transgenesis (Babaryka et al., 2009). These constructs were injected into one-cell-stage wild-type embryos using standard meganuclease transgenesis techniques (Babaryka et al., 2009). To isolate stable lines, larvae were examined for EGFP expression or genotyped for *EGFP* insertions at 1-5 dpf. Twenty-one stable lines were established in this study (listed in Table S9).

RNA-sequencing and analysis

Partial ventricular resection was performed with *tcf21:nucEGFP* animals as described previously (Poss et al., 2002). Ventricles were collected at 3 and 7 dpa together with uninjured clutchmates. Thirty to 50 ventricles per group from fish of mixed sexes were dissociated using Liberase DH (Roche) and EGFP$^+$ epicardial cells were isolated by FACS as described previously (Cao et al., 2016). After FACS sorting, we plated the isolated cells in dishes or on a coverslip and observed >95% purity of EGFP$^+$ cells. We collected 110,000-170,000 cells from each group of two biological replicates. Total RNA was purified using a Qiagen RNeasy Plus Micro Kit. The library was constructed using SMARTer Ultra Low Input RNA Kit for Sequencing and sequencing was performed using an Illumina HiSeq 2000, with 82-94 million 50 bp single-end reads obtained for each library. Sequences were aligned to the zebrafish genome (danRer10) using TopHat2 (Kim et al., 2013). Transcript levels were quantified using HTseq (Anders et al., 2015). Differential expression analysis was carried out using the Bioconductor package DESeq2 (Love et al., 2014).

ATAC sequencing and analysis

Partial ventricular resection was performed with *tcf21:nucEGFP* animals. Ventricles were collected at 3 and 7 dpa together with uninjured clutchmates. Four biological replicates were performed for each group. Ventricle dissociation and epicardial cells isolation were done as described above. ATAC-seq libraries were made from 50,000-198,000 epicardial cells per sample as described previously (Buenrostro et al., 2013). Sequencing was performed using an Illumina HiSeq 2000 with 89-167 million 50-nt single reads obtained for each cell library.

ATAC-seq reads were trimmed for adaptors before aligning to the DanRer10 genome using Bowtie with two mismatches allowed and mapping up to four sites (Langmead et al., 2009). Reads mapped to mitochondrial DNA were removed, and alignments were filtered for PCR artifacts. Peaks were called using MACS v2.1.4 with P<0.01 and shift −37 bp, and extend

73 bp (Zhang et al., 2008). Normalized UCSC browser tracks were generated by conversion of bam format alignments to bp resolution bigWig files and scaling by the total number of mapped reads. The Bioconductor package DiffBind V3.0.15 was used for signal normalization and differential analysis (Ross-Innes et al., 2012). A fold change greater than two and $P<0.05$ were used to filter the significant differential peaks. Genomic distribution of peaks was analyzed using the Bioconductor package ChIPpeakAnno v3.27.2 (Zhu et al., 2010). Packages ChIPpeakAnno (Zhu et al., 2010) and complexHeatmap v2.6.2 (Gu et al., 2016) were used to annotate the peaks and generate heatmaps. The differential peaks were annotated by nearest gene start site to the center of peaks. ATAC-Seq peaks were paired to RNA-Seq differential expression data by annotated nearest gene symbols. Genome-wide motif analysis was performed using HOMER v4.9.1 (Heinz et al., 2010). The motif search of *nrg1*-related sequences was performed using motifmatchr (v 1.12.0) (Schep, 2021) with merged motifs (distance 10 bp) stored in package enhancerHomologSearch (v 1.0.0) (Ou et al., 2021). The dandelionPlot was created by trackViewer v 1.27.15 (Ou and Zhu, 2019). The conserved open-chromatin regions were identified by comparing our dataset with the published zebrafish conserved non-genic elements (zCNEs) database for at least 1 bp overlapped regions (Hiller et al., 2013). Ventricle Chip-seq (H3K27Ac) dataset was downloaded from Gene Expression Omnibus (GEO) under accession number GSE75894.

Histology and microscopy

Freshly collected hearts or larvae were fixed with 4% paraformaldehyde (PFA) for 1.5-2 h at room temperature or overnight at 4°C. Fixed hearts were either mounted with Fluoromount G (Southern Biotechnology, 0100-01) or PBS between two coverslips (allowing imaging of both ventricular surfaces) or applied to 10 µm cryosections. Immunostaining of whole-mounted hearts was carried out as described previously (Cao et al., 2017; Wang et al., 2015). The primary antibody used in this study was mouse anti-EGFP (ThermoFisher, A11120, 1:200). The secondary antibody used in this study was Alexa Fluor 488 goat anti-mouse (ThermoFisher, A11029, 1:200). *In situ* hybridization was performed on 10 µm cryosections of PFA-fixed hearts using digoxigenin-labeled cRNA probes as described previously (Poss et al., 2002). Probes were cloned from 2 dpf zebrafish cDNA using the primers listed in Table S8. Hybridization chain reaction (HCR) was performed using synthesized probes from Molecular Instruments following the published protocols (Choi et al., 2018). Images of fluorescent transgenes in live embryos were captured using a Zeiss Axiozoom V16 microscope. Whole-mount or sectioned heart tissues were imaged using a Zeiss LSM 800 confocal microscope or a Leica DMi8 compound microscope. Whole-mount *in situ* hybridization images of zebrafish embryos were retrieved from the Zebrafish Information Network (ZFIN) (Ruzicka et al., 2019; Thisse et al., 2008).

Acknowledgements

We thank the Zebrafish Core Facility staff at Duke University and Weill Cornell for fish care, and M. Harrison and J. Kang for comments on the manuscript.

Competing interests

The authors declare no competing or financial interests.

Author contributions

Conceptualization: K.D.P., J.C.; Methodology: G.E.C., J.C.; Investigation: Y.C., Y.X., J.J.B., J.O., L.S., A.S., T.C.; Resources: G.E.C., K.D.P., J.C.; Writing - original draft: Y.C.; Writing - review & editing: K.D.P., J.C.; Supervision: K.D.P., J.C.; Project administration: K.D.P., J.C.; Funding acquisition: Y.X., K.D.P., J.C.

Funding

This work was supported by a Rudin Foundation Fellowship to Y.X., by National Institutes of Health (NIH) grants (R01HL131319 and R35HL150713) and an American Heart Association Merit Award to K.D.P., and by an American Heart Association Career Development Award (18CDA34110108), a Weill Cornell Start-up fund and a National Institutes of Health grant (R01HL155607) to J.C. Deposited in PMC for release after 12 months.

Data availability

The RNA-seq and ATAC-seq datasets have been deposited at GEO under accession number GSE89444M.

Peer review history

The peer review history is available online at https://journals.biologists.com/dev/article-lookup/doi/10.1242/dev.200133

References

Anders, S., Pyl, P. T. and Huber, W. (2015). HTSeq–a Python framework to work with high-throughput sequencing data. *Bioinformatics* **31**, 166-169. doi:10.1093/bioinformatics/btu638

Ando, K., Shih, Y. H., Ebarasi, L., Grosse, A., Portman, D., Chiba, A., Mattonet, K., Gerri, C., Stainier, D. Y. R., Mochizuki, N. et al. (2021). Conserved and context-dependent roles for pdgfrb signaling during zebrafish vascular mural cell development. *Dev. Biol.* **479**, 11-22. doi:10.1016/j.ydbio.2021.06.010

Babaryka, A., Kuhn, E. and Koster, R. W. (2009). In vivo synthesis of meganuclease for generating transgenic zebrafish Danio rerio. *J. Fish Biol.* **74**, 452-457. doi:10.1111/j.1095-8649.2008.02075.x

Begeman, I. J., Shin, K., Osorio-Mendez, D., Kurth, A., Lee, N., Chamberlain, T. J., Pelegri, F. J. and Kang, J. (2020). Decoding an organ regeneration switch by dissecting cardiac regeneration enhancers. *Development* **147**, dev194019. doi:10.1242/dev.194019

Beisaw, A., Kuenne, C., Guenther, S., Dallmann, J., Wu, C. C., Bentsen, M., Looso, M. and Stainier, D. Y. R. (2020). AP-1 contributes to chromatin accessibility to promote sarcomere disassembly and cardiomyocyte protrusion during zebrafish heart regeneration. *Circ. Res.* **126**, 1760-1778. doi:10.1161/CIRCRESAHA.119.316167

Buenrostro, J. D., Giresi, P. G., Zaba, L. C., Chang, H. Y. and Greenleaf, W. J. (2013). Transposition of native chromatin for fast and sensitive epigenomic profiling of open chromatin, DNA-binding proteins and nucleosome position. *Nat. Methods* **10**, 1213-1218. doi:10.1038/nmeth.2688

Cao, J. and Poss, K. D. (2018). The epicardium as a hub for heart regeneration. *Nat. Rev. Cardiol* **15**, 631-647. doi:10.1038/s41569-018-0046-4

Cao, J., Navis, A., Cox, B. D., Dickson, A. L., Gemberling, M., Karra, R., Bagnat, M. and Poss, K. D. (2016). Single epicardial cell transcriptome sequencing identifies Caveolin 1 as an essential factor in zebrafish heart regeneration. *Development* **143**, 232-243. doi:10.1242/dev.130534

Cao, J., Wang, J., Jackman, C. P., Cox, A. H., Trembley, M. A., Balowski, J. J., Cox, B. D., De Simone, A., Dickson, A. L., Di Talia, S. et al. (2017). Tension creates an endoreplication wavefront that leads regeneration of epicardial tissue. *Dev. Cell* **42**, 600-615. doi:10.1016/j.devcel.2017.08.024

Chablais, F. and Jazwinska, A. (2012). The regenerative capacity of the zebrafish heart is dependent on TGFbeta signaling. *Development* **139**, 1921-1930. doi:10.1242/dev.078543

Chen, A., Han, Y. and Poss, K. D. (2020). Regulation of zebrafish fin regeneration by vitamin D signaling. *Dev. Dyn.* **250**, 1330-1339. doi:10.1002/dvdy.261

Choi, W. Y., Gemberling, M., Wang, J., Holdway, J. E., Shen, M. C., Karlstrom, R. O. and Poss, K. D. (2013). In vivo monitoring of cardiomyocyte proliferation to identify chemical modifiers of heart regeneration. *Development* **140**, 660-666. doi:10.1242/dev.088526

Choi, H. M. T., Schwarzkopf, M., Fornace, M. E., Acharya, A., Artavanis, G., Stegmaier, J., Cunha, A. and Pierce, N. A. (2018). Third-generation in situ hybridization chain reaction: multiplexed, quantitative, sensitive, versatile, robust. *Development* **145**, dev165753. doi:10.1242/dev.165753

Choi, J., Lysakovskaia, K., Stik, G., Demel, C., Soding, J., Tian, T. V., Graf, T. and Cramer, P. (2021). Evidence for additive and synergistic action of mammalian enhancers during cell fate determination. *eLife* **10**, e65381. doi:10.7554/eLife.65381

Crespillo, D. I. C., Ester, M. and Torres, M. (2021). The role of Meis transcription factors in the epicardium.

de Bakker, D. E. M., Bouwman, M., Dronkers, E., Simoes, F. C., Riley, P. R., Goumans, M. J., Smits, A. M. and Bakkers, J. (2021). Prrx1b restricts fibrosis and promotes Nrg1-dependent cardiomyocyte proliferation during zebrafish heart regeneration. *Development* **148**, dev198937. doi:10.1242/dev.198937

Dickel, D. E., Ypsilanti, A. R., Pla, R., Zhu, Y., Barozzi, I., Mannion, B. J., Khin, Y. S., Fukuda-Yuzawa, Y., Plajzer-Frick, I., Pickle, C. S. et al. (2018). Ultraconserved enhancers are required for normal development. *Cell* **172**, 491-499. doi:10.1016/j.cell.2017.12.017

Duncan, B. W., Murphy, K. E. and Maness, P. F. (2021). Molecular mechanisms of L1 and NCAM adhesion molecules in synaptic pruning, plasticity, and stabilization. *Front. Cell Dev. Biol.* **9**, 625340. doi:10.3389/fcell.2021.625340

Dunipace, L., Akos, Z. and Stathopoulos, A. (2019). Coacting enhancers can have complementary functions within gene regulatory networks and promote canalization. *PLoS Genet.* **15**, e1008525. doi:10.1371/journal.pgen.1008525

Feng, T., Meng, J., Kou, S., Jiang, Z., Huang, X., Lu, Z., Zhao, H., Lau, L. F., Zhou, B. and Zhang, H. (2019). CCN1-Induced cellular senescence promotes heart regeneration. *Circulation* **139**, 2495-2498. doi:10.1161/CIRCULATIONAHA.119.039530

Fivaz, J., Bassi, M. C., Pinaud, S. and Mirkovitch, J. (2000). RNA polymerase II promoter-proximal pausing upregulates c-fos gene expression. *Gene* **255**, 185-194. doi:10.1016/S0378-1119(00)00340-1

Gemberling, M., Karra, R., Dickson, A. L. and Poss, K. D. (2015). Nrg1 is an injury-induced cardiomyocyte mitogen for the endogenous heart regeneration program in zebrafish. *eLife* **4**, e05871. doi:10.7554/eLife.05871.015

Goldman, J. A., Kuzu, G., Lee, N., Karasik, J., Gemberling, M., Foglia, M. J., Karra, R., Dickson, A. L., Sun, F., Tolstorukov, M. Y. et al. (2017). Resolving heart regeneration by replacement histone profiling. *Dev. Cell* **40**, 392-404. doi:10.1016/j.devcel.2017.01.013

Gonzalez-Rosa, J. M., Peralta, M. and Mercader, N. (2012). Pan-epicardial lineage tracing reveals that epicardium derived cells give rise to myofibroblasts and perivascular cells during zebrafish heart regeneration. *Dev. Biol.* **370**, 173-186. doi:10.1016/j.ydbio.2012.07.007

Gu, Z., Eils, R. and Schlesner, M. (2016). Complex heatmaps reveal patterns and correlations in multidimensional genomic data. *Bioinformatics* **32**, 2847-2849. doi:10.1093/bioinformatics/btw313

Harris, R. E., Setiawan, L., Saul, J. and Hariharan, I. K. (2016). Localized epigenetic silencing of a damage-activated WNT enhancer limits regeneration in mature Drosophila imaginal discs. *eLife* **5**, e11588. doi:10.7554/eLife.11588.028

Heinz, S., Benner, C., Spann, N., Bertolino, E., Lin, Y. C., Laslo, P., Cheng, J. X., Murre, C., Singh, H. and Glass, C. K. (2010). Simple combinations of lineage-determining transcription factors prime cis-regulatory elements required for macrophage and B cell identities. *Mol. Cell* **38**, 576-589. doi:10.1016/j.molcel.2010.05.004

Hiller, M., Agarwal, S., Notwell, J. H., Parikh, R., Guturu, H., Wenger, A. M. and Bejerano, G. (2013). Computational methods to detect conserved non-genic elements in phylogenetically isolated genomes: application to zebrafish. *Nucleic Acids Res.* **41**, e151. doi:10.1093/nar/gkt557

Hnisz, D., Abraham, B. J., Lee, T. I., Lau, A., Saint-Andre, V., Sigova, A. A., Hoke, H. A. and Young, R. A. (2013). Super-enhancers in the control of cell identity and disease. *Cell* **155**, 934-947. doi:10.1016/j.cell.2013.09.053

Hu, H., Lin, S., Wang, S. and Chen, X. (2020). The role of transcription factor 21 in epicardial cell differentiation and the development of coronary heart disease. *Front Cell Dev Biol* **8**, 457. doi:10.3389/fcell.2020.00457

Huang, G. N., Thatcher, J. E., McAnally, J., Kong, Y., Qi, X., Tan, W., DiMaio, J. M., Amatruda, J. F., Gerard, R. D., Hill, J. A. et al. (2012). C/EBP transcription factors mediate epicardial activation during heart development and injury. *Science* **338**, 1599-1603. doi:10.1126/science.1229765

Hui, S. P., Sheng, D. Z., Sugimoto, K., Gonzalez-Rajal, A., Nakagawa, S., Hesselson, D. and Kikuchi, K. (2017). Zebrafish regulatory T cells mediate organ-specific regenerative programs. *Dev. Cell* **43**, 659-672. doi:10.1016/j.devcel.2017.11.010

Kang, J., Hu, J., Karra, R., Dickson, A. L., Tornini, V. A., Nachtrab, G., Gemberling, M., Goldman, J. A., Black, B. L. and Poss, K. D. (2016). Modulation of tissue repair by regeneration enhancer elements. *Nature* **532**, 201-206. doi:10.1038/nature17644

Karra, R., Foglia, M. J., Choi, W.-Y., Belliveau, C., DeBenedittis, P. and Poss, K. D. (2018). Vegfaa instructs cardiac muscle hyperplasia in adult zebrafish. *Proc. Natl. Acad. Sci. USA* **115**, 8805-8810. doi:10.1073/pnas.1722594115

Kikuchi, K., Gupta, V., Wang, J., Holdway, J. E., Wills, A. A., Fang, Y. and Poss, K. D. (2011a). tcf21+ epicardial cells adopt non-myocardial fates during zebrafish heart development and regeneration. *Development* **138**, 2895-2902. doi:10.1242/dev.067041

Kikuchi, K., Holdway, J. E., Major, R. J., Blum, N., Dahn, R. D., Begemann, G. and Poss, K. D. (2011b). Retinoic acid production by endocardium and epicardium is an injury response essential for zebrafish heart regeneration. *Dev. Cell* **20**, 397-404. doi:10.1016/j.devcel.2011.01.010

Kim, D., Pertea, G., Trapnell, C., Pimentel, H., Kelley, R. and Salzberg, S. L. (2013). TopHat2: accurate alignment of transcriptomes in the presence of insertions, deletions and gene fusions. *Genome Biol.* **14**, R36. doi:10.1186/gb-2013-14-4-r36

Kolander, K. D., Holtz, M. L., Cossette, S. M., Duncan, S. A. and Misra, R. P. (2014). Epicardial GATA factors regulate early coronary vascular plexus formation. *Dev. Biol.* **386**, 204-215. doi:10.1016/j.ydbio.2013.12.033

Koth, J., Wang, X., Killen, A. C., Stockdale, W. T., Potts, H. G., Jefferson, A., Bonkhofer, F., Riley, P. R., Patient, R. K., Gottgens, B. et al. (2020). Runx1 promotes scar deposition and inhibits myocardial proliferation and survival during zebrafish heart regeneration. *Development* **147**, dev186569. doi:10.1242/dev.186569

Kvon, E. Z., Waymack, R., Gad, M. and Wunderlich, Z. (2021). Enhancer redundancy in development and disease. *Nat. Rev. Genet.* **22**, 324-336. doi:10.1038/s41576-020-00311-x

Langmead, B., Trapnell, C., Pop, M. and Salzberg, S. L. (2009). Ultrafast and memory-efficient alignment of short DNA sequences to the human genome. *Genome Biol.* **10**, R25. doi:10.1186/gb-2009-10-3-r25

Lee, H. J., Hou, Y., Chen, Y., Dailey, Z. Z., Riddihough, A., Jang, H. S., Wang, T. and Johnson, S. L. (2020). Regenerating zebrafish fin epigenome is characterized by stable lineage-specific DNA methylation and dynamic chromatin accessibility. *Genome Biol.* **21**, 52. doi:10.1186/s13059-020-1948-0

Lepilina, A., Coon, A. N., Kikuchi, K., Holdway, J. E., Roberts, R. W., Burns, C. G. and Poss, K. D. (2006). A dynamic epicardial injury response supports progenitor cell activity during zebrafish heart regeneration. *Cell* **127**, 607-619. doi:10.1016/j.cell.2006.08.052

Liu, J., Wang, W., Liu, M., Su, L., Zhou, H., Xia, Y., Ran, J., Lin, H. Y. and Yang, B. (2016). Repulsive guidance molecule b inhibits renal cyst development through the bone morphogenetic protein signaling pathway. *Cell. Signal.* **28**, 1842-1851. doi:10.1016/j.cellsig.2016.08.015

Love, M. I., Huber, W. and Anders, S. (2014). Moderated estimation of fold change and dispersion for RNA-seq data with DESeq2. *Genome Biol.* **15**, 550. doi:10.1186/s13059-014-0550-8

Lu, H. and Huang, H. (2011). FOXO1: a potential target for human diseases. *Curr. Drug Targets* **12**, 1235-1244. doi:10.2174/138945011796150280

Marin-Juez, R., El-Sammak, H., Helker, C. S. M., Kamezaki, A., Mullapuli, S. T., Bibli, S. I., Foglia, M. J., Fleming, I., Poss, K. D. and Stainier, D. Y. R. (2019). Coronary revascularization during heart regeneration is regulated by epicardial and endocardial cues and forms a scaffold for cardiomyocyte repopulation. *Dev. Cell* **51**, 503-515. doi:10.1016/j.devcel.2019.10.019

Masters, M. and Riley, P. R. (2014). The epicardium signals the way towards heart regeneration. *Stem Cell Res.* **13**, 683-692. doi:10.1016/j.scr.2014.04.007

Nakae, J., Kitamura, T., Silver, D. L. and Accili, D. (2001). The forkhead transcription factor Foxo1 (Fkhr) confers insulin sensitivity onto glucose-6-phosphatase expression. *J. Clin. Invest.* **108**, 1359-1367. doi:10.1172/JCI200112876

Nieto-Arellano, R. and Sanchez-Iranzo, H. (2019). zfRegeneration: a database for gene expression profiling during regeneration. *Bioinformatics* **35**, 703-705. doi:10.1093/bioinformatics/bty659

Osterwalder, M., Barozzi, I., Tissieres, V., Fukuda-Yuzawa, Y., Mannion, B. J., Afzal, S. Y., Lee, E. A., Zhu, Y., Plajzer-Frick, I., Pickle, C. S. et al. (2018). Enhancer redundancy provides phenotypic robustness in mammalian development. *Nature* **554**, 239-243. doi:10.1038/nature25461

Ou, J. and Zhu, L. J. (2019). trackViewer: a Bioconductor package for interactive and integrative visualization of multi-omics data. *Nat. Methods* **16**, 453-454. doi:10.1038/s41592-019-0430-y

Ou, J., Cigliola, V. and Poss, K. D. (2021). enhancerHomologSearch: Identification of putative mammalian orthologs to given enhancer. *R package version 1.0.0*.

Pennacchio, L. A., Bickmore, W., Dean, A., Nobrega, M. A. and Bejerano, G. (2013). Enhancers: five essential questions. *Nat. Rev. Genet.* **14**, 288-295. doi:10.1038/nrg3458

Pfefferli, C. and Jazwinska, A. (2017). The careg element reveals a common regulation of regeneration in the zebrafish myocardium and fin. *Nat. Commun.* **8**, 15151. doi:10.1038/ncomms15151

Poss, K. D., Wilson, L. G. and Keating, M. T. (2002). Heart regeneration in zebrafish. *Science* **298**, 2188-2190. doi:10.1126/science.1077857

Ross-Innes, C. S., Stark, R., Teschendorff, A. E., Holmes, K. A., Ali, H. R., Dunning, M. J., Brown, G. D., Gojis, O., Ellis, I. O., Green, A. R. et al. (2012). Differential oestrogen receptor binding is associated with clinical outcome in breast cancer. *Nature* **481**, 389-393. doi:10.1038/nature10730

Ruzicka, L., Howe, D. G., Ramachandran, S., Toro, S., Van Slyke, C. E., Bradford, Y. M., Eagle, A., Fashena, D., Frazer, K., Kalita, P. et al. (2019). The Zebrafish information network: new support for non-coding genes, richer gene ontology annotations and the alliance of genome resources. *Nucleic Acids Res.* **47**, D867-D873. doi:10.1093/nar/gky1090

Samad, T. A., Rebbapragada, A., Bell, E., Zhang, Y., Sidis, Y., Jeong, S. J., Campagna, J. A., Perusini, S., Fabrizio, D. A., Schneyer, A. L. et al. (2005). DRAGON, a bone morphogenetic protein co-receptor. *J. Biol. Chem.* **280**, 14122-14129. doi:10.1074/jbc.M410034200

Sarig, R., Rimmer, R., Bassat, E., Zhang, L., Umansky, K. B., Lendengolts, D., Perlmoter, G., Yaniv, K. and Tzahor, E. (2019). Transient p53-mediated regenerative senescence in the injured heart. *Circulation* **139**, 2491-2494. doi:10.1161/CIRCULATIONAHA.119.040125

Schep, A. (2021). motifmatchr: Fast Motif Matching in R. *R package version 1.16.0*.

Siles, A. M., Martinez-Hernandez, E., Araque, J., Diaz-Manera, J., Rojas-Garcia, R., Gallardo, E., Illa, I., Graus, F. and Querol, L. (2018). Antibodies against cell adhesion molecules and neural structures in paraneoplastic neuropathies. *Ann Clin Transl Neurol* **5**, 559-569. doi:10.1002/acn3.554

Sugimoto, K., Hui, S. P., Sheng, D. Z. and Kikuchi, K. (2017). Dissection of zebrafish shha function using site-specific targeting with a Cre-dependent genetic switch. *eLife* **6**, e24635. doi:10.7554/eLife.24635.021

Syrovatkina, V., Alegre, K. O., Dey, R. and Huang, X.-Y. (2016). Regulation, signaling, and physiological functions of G-proteins. *J. Mol. Biol.* **428**, 3850-3868. doi:10.1016/j.jmb.2016.08.002

Thisse, B. and Thisse, C. (2004). Fast release clones: a high throughput expression analysis. *ZFIN Direct Data Submission*, https://zfin.org/ZDB-PUB-040907-1

Thisse, B., Wright, G. J. and Thisse, C. (2008). Embryonic and larval expression patterns from a large scale screening for novel low affinity extracellular protein interactions. *ZFIN Direct Data Submission*, https://zfin.org/ZDB-PUB-040907-1

Thompson, J. D., Ou, J., Lee, N., Shin, K., Cigliola, V., Song, L., Crawford, G. E., Kang, J. and Poss, K. D. (2020). Identification and requirements of enhancers that direct gene expression during zebrafish fin regeneration. *Development* **147**, dev191262. doi:10.1242/dev.191262

Umer, H. M., Smolinska-Garbulowska, K., Marzouka, N.-a.-d., Khaliq, Z., Wadelius, C. and Komorowski, J. (2019). funMotifs: Tissue-specific transcription factor motifs. *bioRxiv* 683722. doi:10.1101/683722

van Duijvenboden, K., de Bakker, D. E. M., Man, J. C. K., Janssen, R., Gunthel, M., Hill, M. C., Hooijkaas, I. B., van der Made, I., van der Kraak, P. H., Vink, A. et al. (2019). Conserved NPPB+ border zone switches from MEF2- to AP-1-driven gene program. *Circulation* **140**, 864-879. doi:10.1161/CIRCULATIONAHA.118.038944

Vizcaya-Molina, E., Klein, C. C., Serras, F., Mishra, R. K., Guigo, R. and Corominas, M. (2018). Damage-responsive elements in Drosophila regeneration. *Genome Res.* **28**, 1852-1866. doi:10.1101/gr.233098.11

Wang, J., Karra, R., Dickson, A. L. and Poss, K. D. (2013). Fibronectin is deposited by injury-activated epicardial cells and is necessary for zebrafish heart regeneration. *Dev. Biol.* **382**, 427-435. doi:10.1016/j.ydbio.2013.08.012

Wang, J., Cao, J., Dickson, A. L. and Poss, K. D. (2015). Epicardial regeneration is guided by cardiac outflow tract and Hedgehog signalling. *Nature* **522**, 226-230. doi:10.1038/nature14325

Wang, J., Panáková, D., Kikuchi, K., Holdway, J. E., Gemberling, M., Burris, J. S., Singh, S. P., Dickson, A. L., Lin, Y.-F., Sabeh, M. K. et al. (2011). The regenerative capacity of zebrafish reverses cardiac failure caused by genetic cardiomyocyte depletion. *Development* **138**, 3421-3430. doi:10.1242/dev.068601

Wang, Y., Zhou, Y. and Graves, D. T. (2014). FOXO transcription factors: their clinical significance and regulation. *Biomed Res Int* **2014**, 925350. doi:10.1155/2014/925350

Wang, W., Hu, C. K., Zeng, A., Alegre, D., Hu, D., Gotting, K., Ortega Granillo, A., Wang, Y., Robb, S., Schnittker, R. et al. (2020). Changes in regeneration-responsive enhancers shape regenerative capacities in vertebrates. *Science* **369**, eaaz3090. doi:10.1126/science.aaz3090

Wei, K., Serpooshan, V., Hurtado, C., Diez-Cunado, M., Zhao, M., Maruyama, S., Zhu, W., Fajardo, G., Noseda, M., Nakamura, K. et al. (2015). Epicardial FSTL1 reconstitution regenerates the adult mammalian heart. *Nature* **525**, 479-485. doi:10.1038/nature15372

Weinberger, M., Simoes, F. C., Patient, R., Sauka-Spengler, T. and Riley, P. R. (2020). Functional heterogeneity within the developing Zebrafish epicardium. *Dev. Cell* **52**, 574-590. doi:10.1016/j.devcel.2020.01.023

Weinberger, M., Simões, F. C., Sauka-Spengler, T. and Riley, P. R. (2021). Distinct epicardial gene regulatory programmes drive development and regeneration of the zebrafish heart. *bioRxiv* 2021.2006.2029.450229. doi:10.1101/2021.06.29.450229

Wu, C. C., Kruse, F., Vasudevarao, M. D., Junker, J. P., Zebrowski, D. C., Fischer, K., Noel, E. S., Grun, D., Berezikov, E., Engel, F. B. et al. (2016). Spatially resolved genome-wide transcriptional profiling identifies bmp signaling as essential regulator of Zebrafish cardiomyocyte regeneration. *Dev. Cell* **36**, 36-49. doi:10.1016/j.devcel.2015.12.010

Xiao, Y., Hill, M. C., Zhang, M., Martin, T. J., Morikawa, Y., Wang, S., Moise, A. R., Wythe, J. D. and Martin, J. F. (2018). Hippo signaling plays an essential role in cell state transitions during cardiac fibroblast development. *Dev. Cell* **45**, 153-169. doi:10.1016/j.devcel.2018.03.019

Yan, C., Xu, Z. and Huang, W. (2021). Cellular senescence affects cardiac regeneration and repair in ischemic heart disease. *Aging Dis* **12**, 552-569. doi:10.14336/AD.2020.0811

Zhang, Y., Liu, T., Meyer, C. A., Eeckhoute, J., Johnson, D. S., Bernstein, B. E., Nusbaum, C., Myers, R. M., Brown, M., Li, W. et al. (2008). Model-based analysis of ChIP-Seq (MACS). *Genome Biol.* **9**, R137. doi:10.1186/gb-2008-9-9-r137

Zhu, L. J., Gazin, C., Lawson, N. D., Pages, H., Lin, S. M., Lapointe, D. S. and Green, M. R. (2010). ChIPpeakAnno: a Bioconductor package to annotate ChIP-seq and ChIP-chip data. *BMC Bioinformatics* **11**, 237. doi:10.1186/1471-2105-11-237

Figure S1

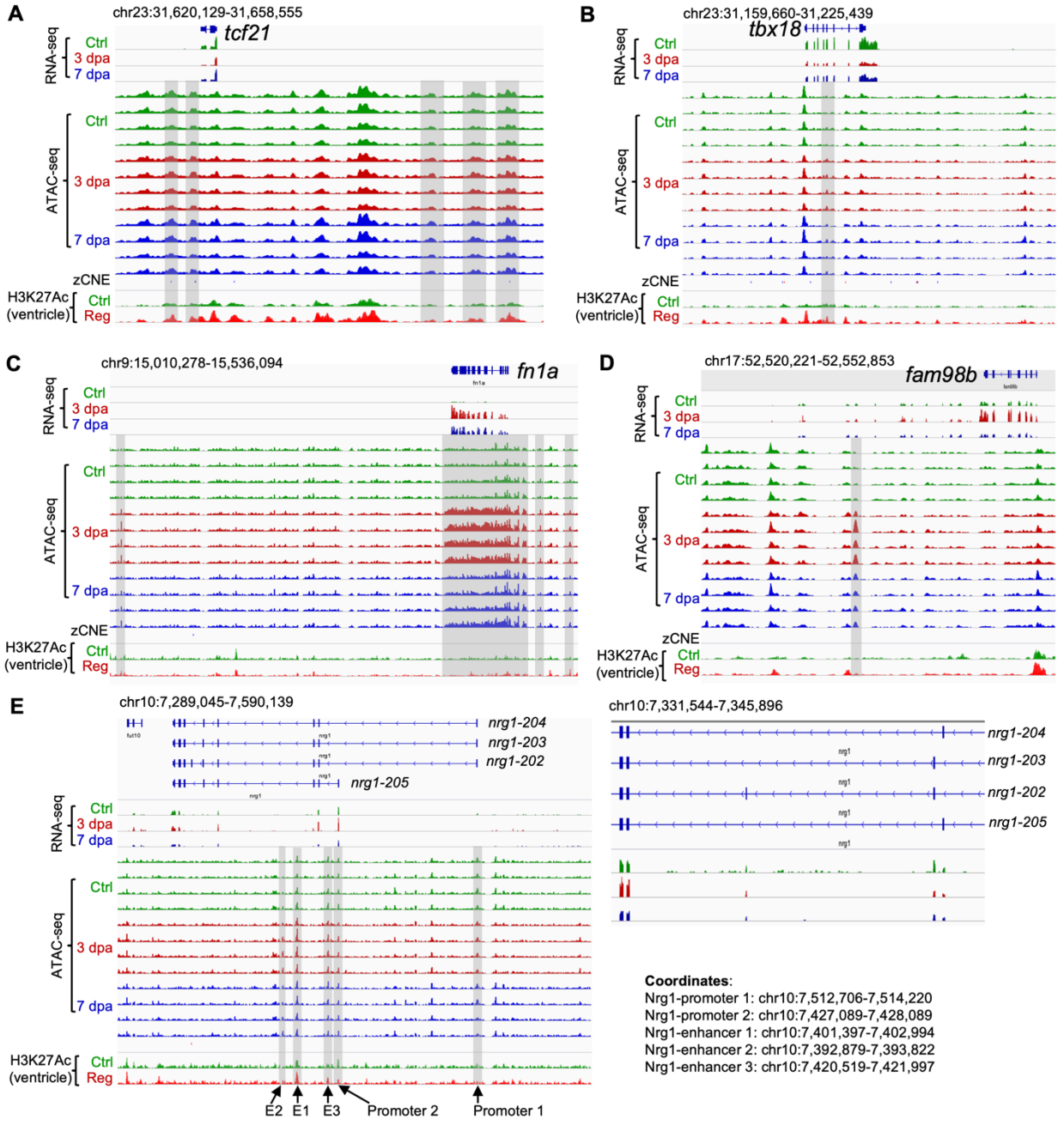

Fig. S1. Browser tracks of the genomic regions comprising *tcf21*, *tbx18*, *fn1a*, *fam98b*, or *nrg1*. Chromatin accessibility profiles in the epicardium, the zCNE sites, and the whole-ventricle H3K27Ac profile are shown. Selected putative enhancer regions or promoters are highlighted in gray boxes. Four *nrg1* isoforms are shown. Two promoters and three putative enhancers (E1-E3) region are marked with the coordinates shown on the bottom right.

Figure S2

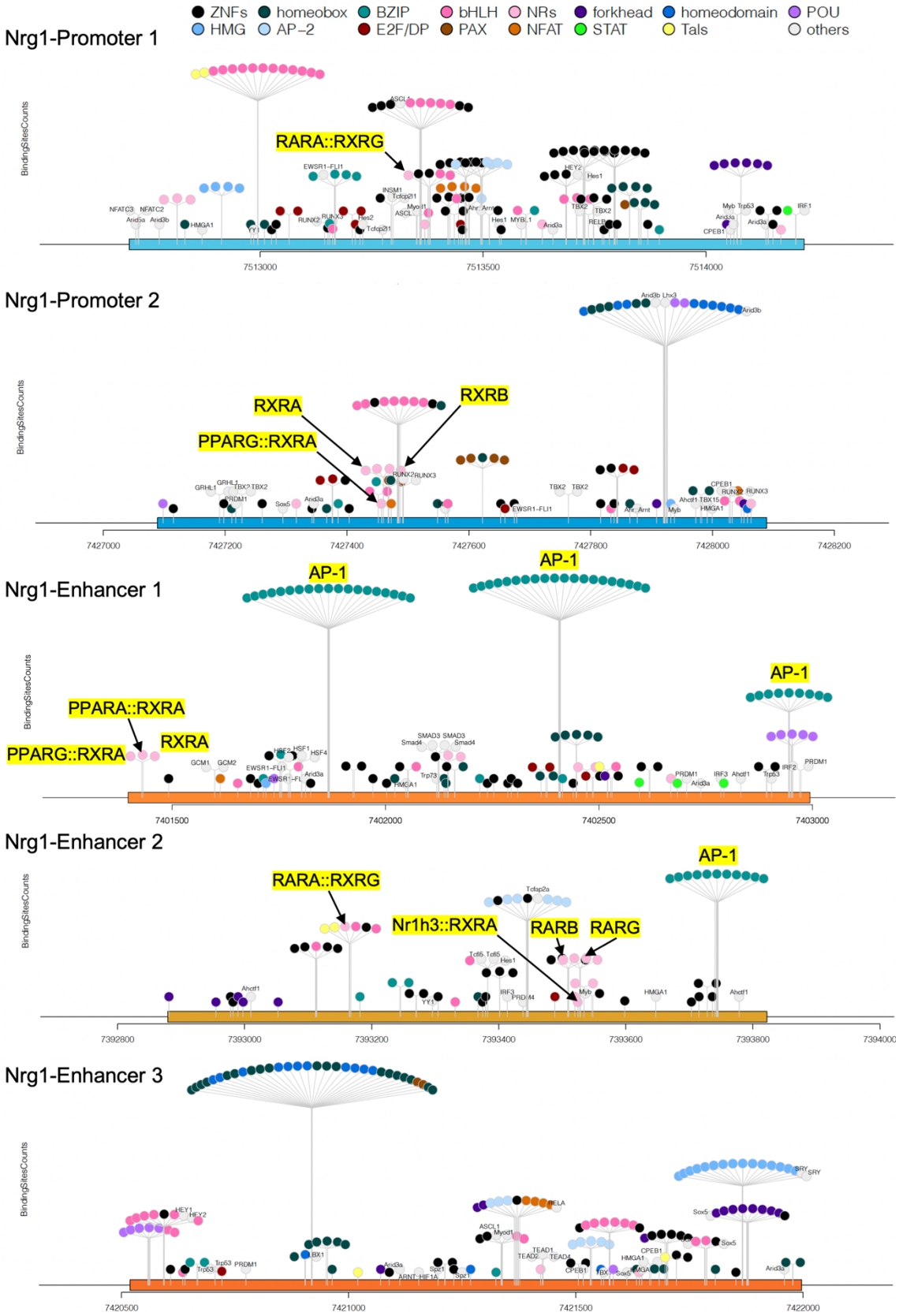

Fig. S2. Motif search results of *nrg1* promoters and putative enhancers. AP-1 complex, Retinoid X Receptor, and Retinoic Acid Receptor binding sites are highlighted. Refer to Table S3 for details.

Figure S3

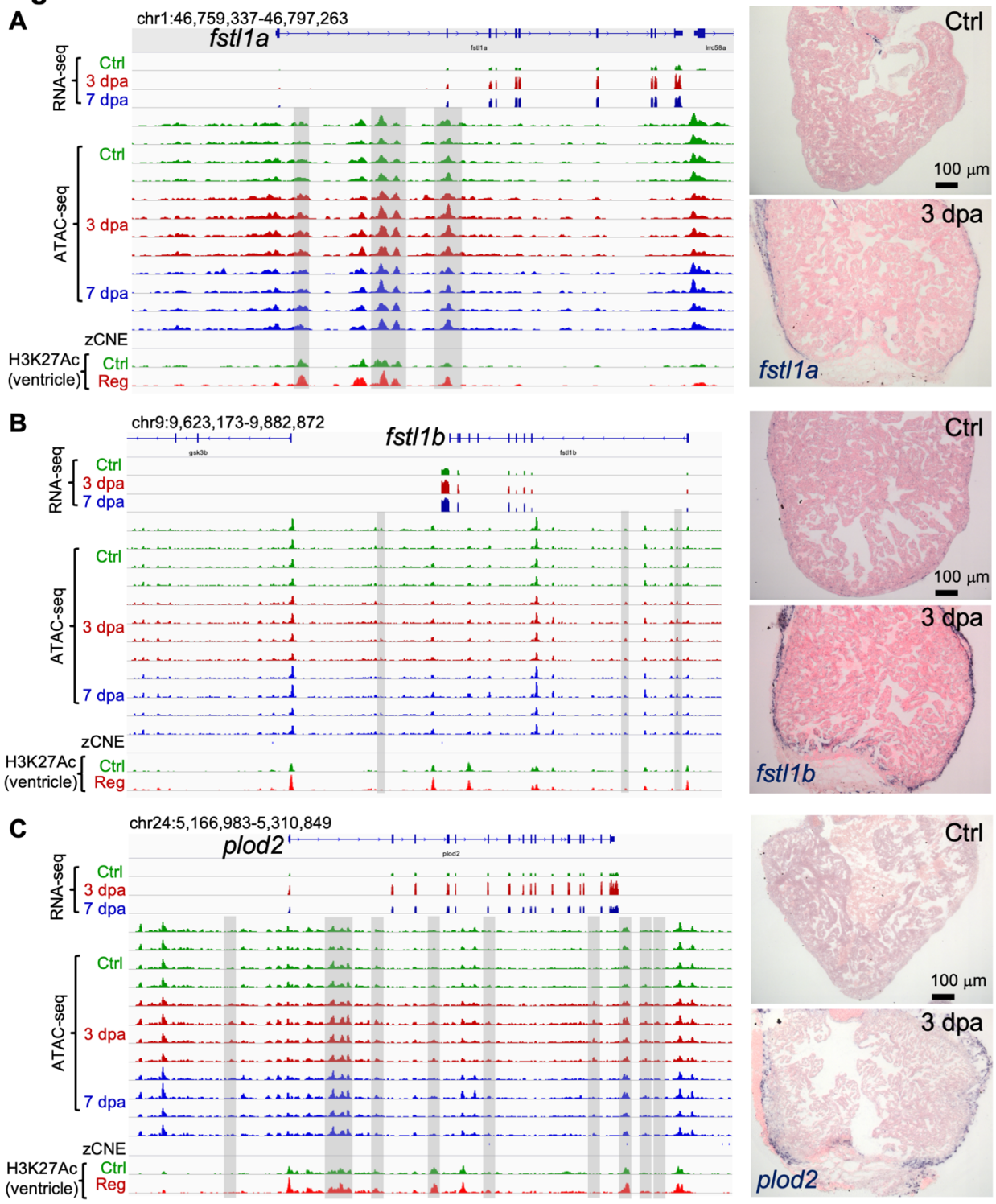

Figure S3-continued

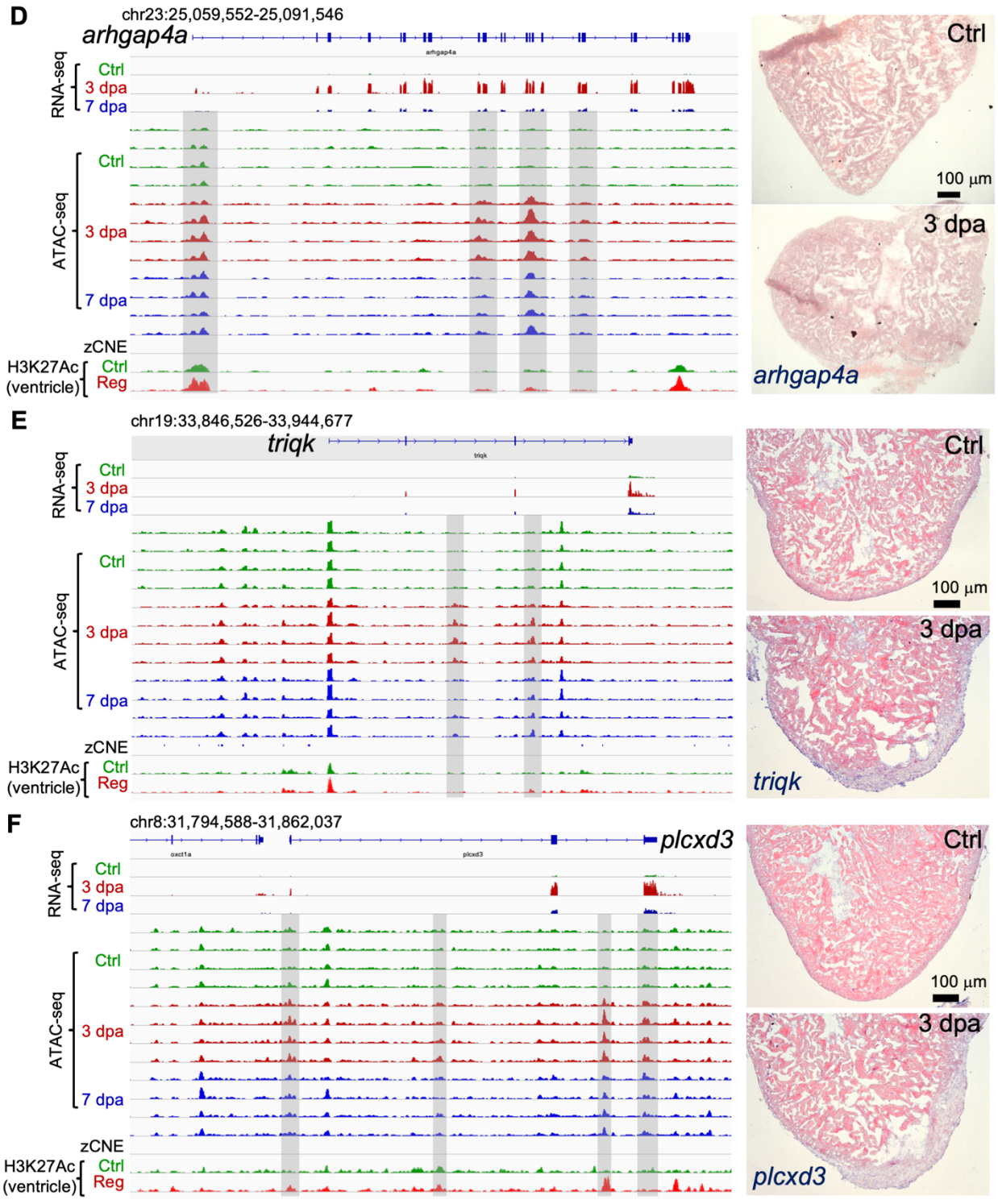

Fig. S3. Browser tracks of the genomic regions and *in situ* hybridization results. Chromatin accessibility profiles in the epicardium, the zCNE sites, and the whole-ventricle H3K27Ac profile are shown. Selected putative enhancer regions are highlighted in gray boxes. *In situ* hybridizations were performed on ventricular sections of uninjured (Ctrl) adult hearts or hearts collected at 3 dpa. Gene expressions in the epicardium were detected upon injury for *fstl1a*, *fstl1b*, *plod2*, *triqk*, and *plcxd3*. Scar bars, 100 μm.

Figure S4

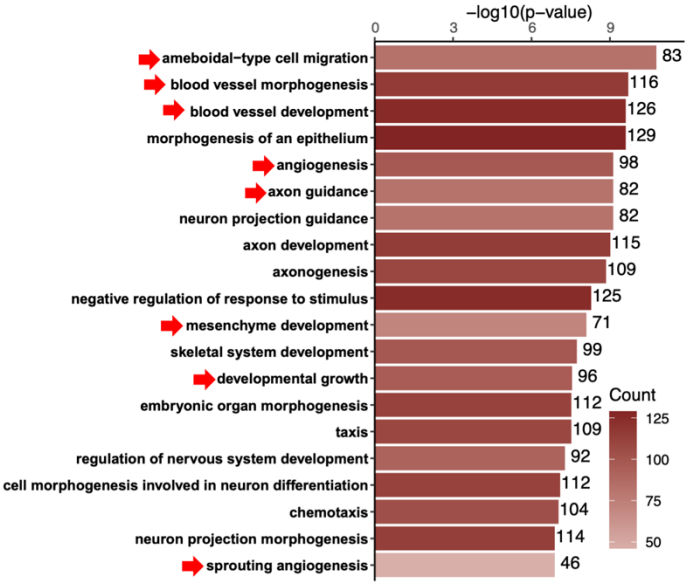

Fig. S4. Barplot showing the 20 most enriched GO biological function terms obtained from peaks with increased chromatin accessibility in 3 dpa samples (FDR < 0.01). The full list is shown in Table S5.

Figure S5

ncam1a

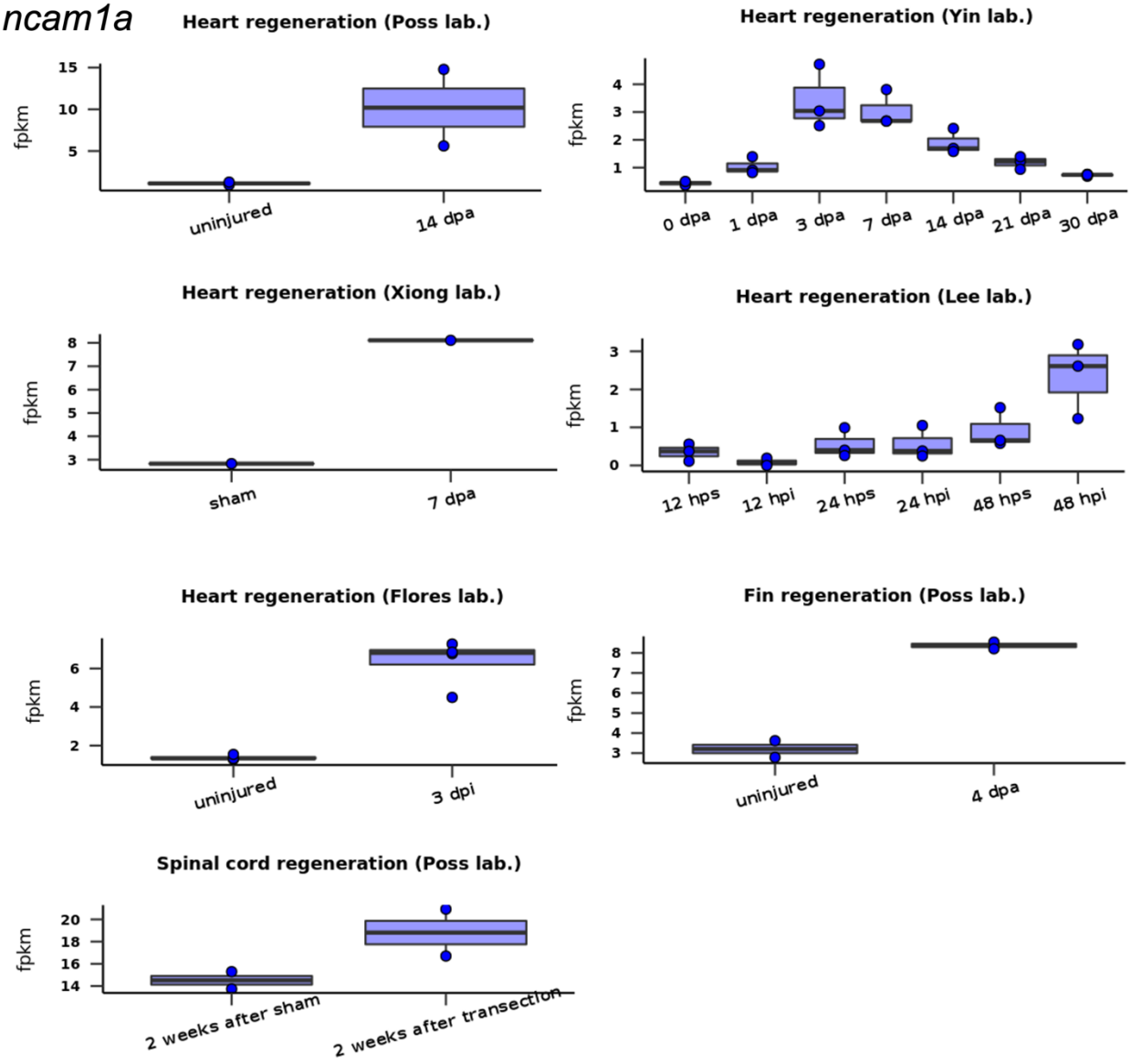

Fig. S5. *ncam1a* expression during zebrafish heart, fin, or spinal cord regeneration.

Plots were generated using the Zebrafish Regeneration Database.

Figure S6

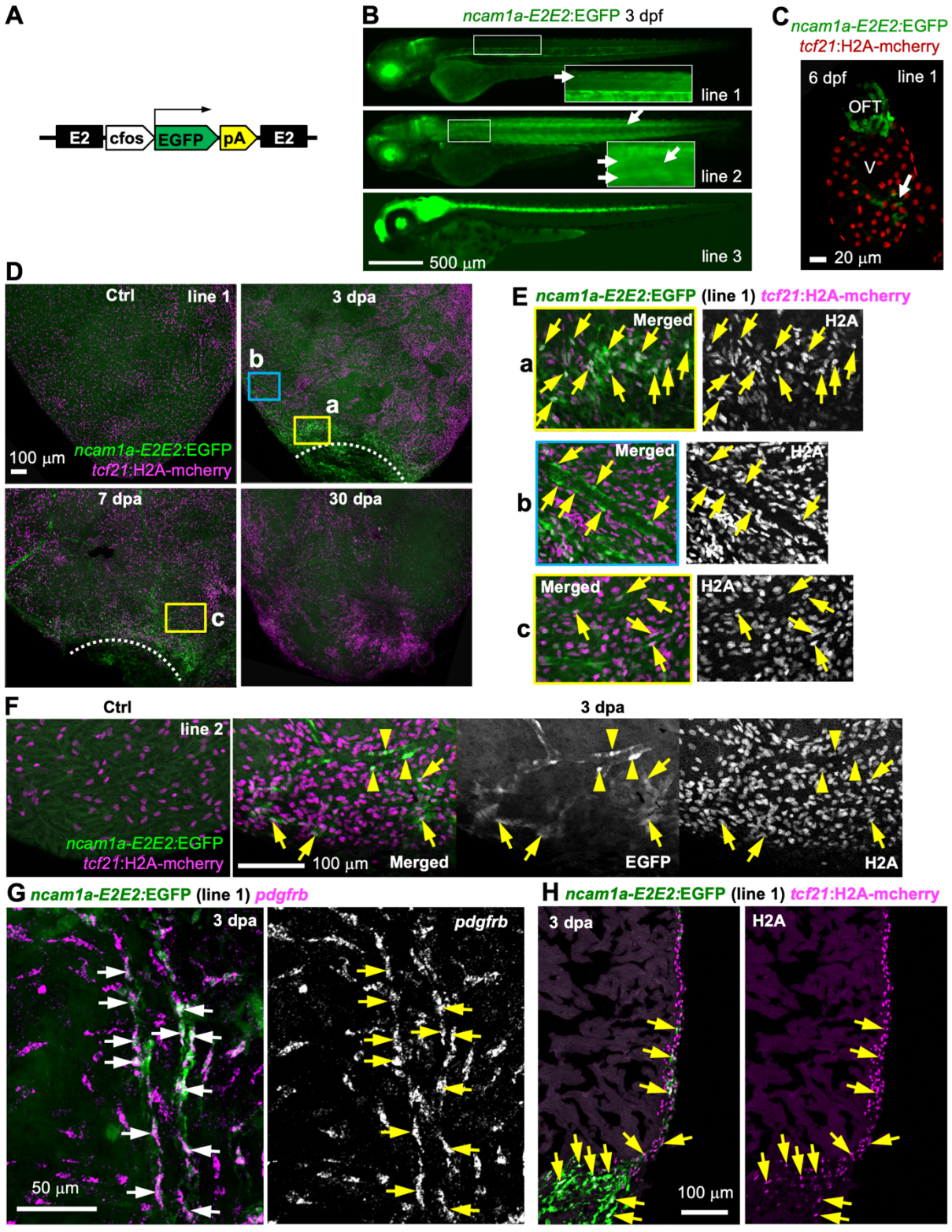

Fig. S6. *ncam1a-E2E2* directs injury-induced epicardial gene expression.

(A) The *ncam1a-E2E2:EGFP* enhancer reporter construct. A second *ncam1a-E2* enhancer was placed after the poly-A sequence. **(B)** Larval expression of the *ncam1a-E2E2:EGFP* lines. Besides the eye, brain, spinal cord, and notochord expressions, additional EGFP signals are detected in the skeletal muscle for line 2. Scale bar, 500 μm. **(C)** Whole-mount images of a 6 dpf heart showing EGFP expression in the outflow tract (OFT) and the atrioventricular valves (arrows). *tcf21*:H2A-mCherry (red) labels the epicardial cells. V, ventricle. Scale bar, 20 μm. **(D)** Whole-mount images (maximum projections) of the ventricular surface showing expressions of *ncam1a-E2E2:EGFP* line 1 (green) in uninjured (Ctrl) and 3, 7, and 30 dpa samples. *tcf21*:H2A-mCherry (magenta) labels the epicardial cells. White dashed lines indicate the injury sites. The framed regions are enlarged to show details in (E). Scale bar, 100 μm. **(E)** Single optical section images of the framed regions in (D). Single-channel images are shown in grayscale. Arrows indicate representative $GFP^+mCherry^+$ cells. Double-positive perivascular cells are shown in (b) and (c). **(F)** Whole-mount images showing expressions of *ncam1a-E2E2:EGFP* line 2 (green) in uninjured (Ctrl) and 3 dpa samples. *tcf21*:H2A-mCherry (magenta) labels the epicardial cells. Single-channel images of the 3 dpa sample are shown in grayscale. Arrowheads (perivascular cells) and arrows indicate representative $EGFP^+mCherry^+$ cells. Scale bar, 100 μm. **(G)** HCR staining result of *pdgfrb* (magenta) on a whole-mounted heart carrying the *ncam1a-E2E2:EGFP* reporter (line 1, green). Single-channel image shows staining signals of *pdgfrb*. Arrows denote $EGFP^+$*pdgfrb*$^+$ cells. Scale bar, 50 μm. **(H)** Section images demonstrating expressions of *ncam1a-E2E2:EGFP* (green) in *tcf21*:H2A-$mCherry^+$ (magenta) cells. Arrows denote representative double-positive cells. Scale bar, 100 μm.

Figure S7

rgmb

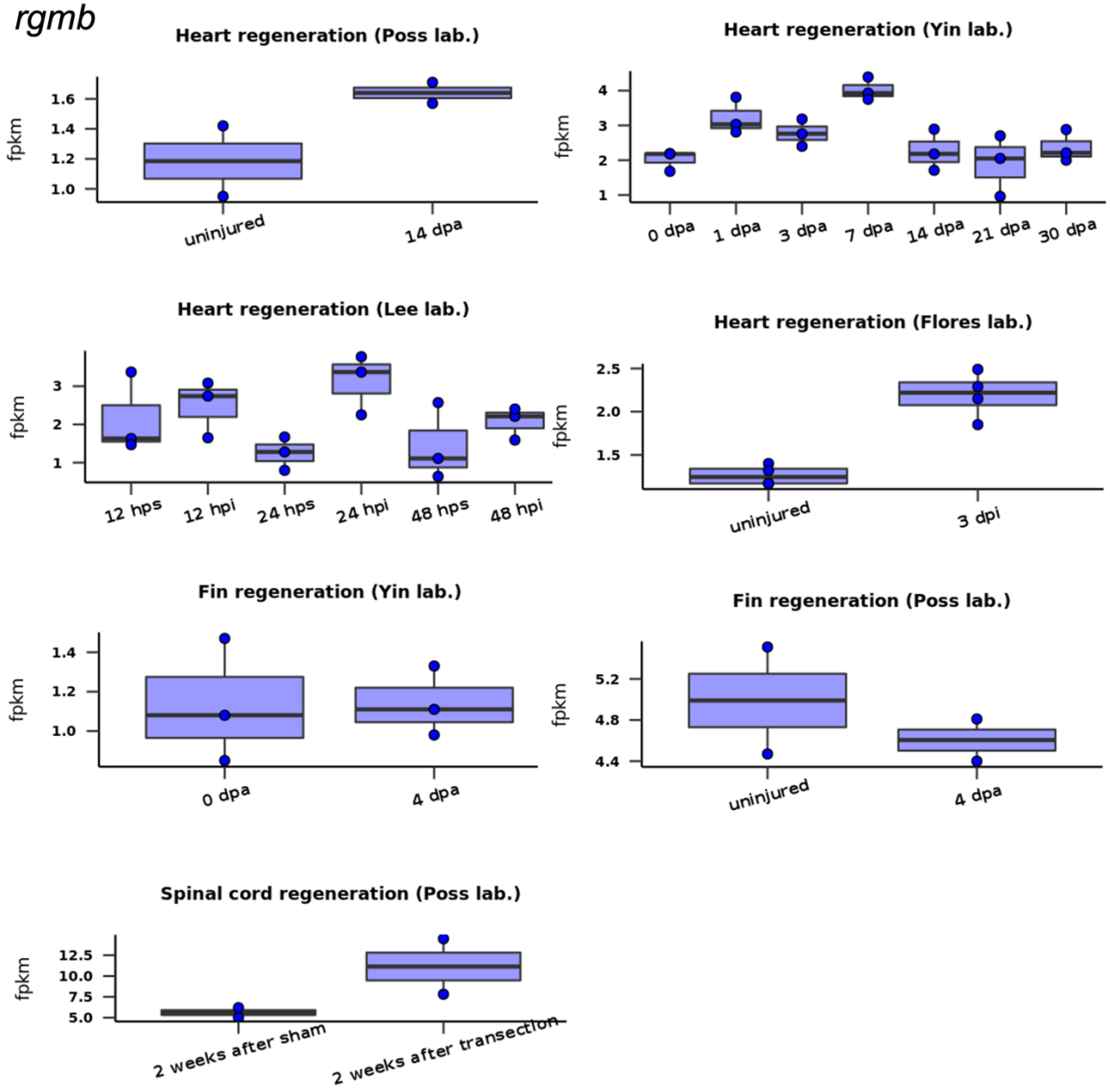

Fig. S7. *rgmb* expression during zebrafish heart, fin, or spinal cord regeneration.

Plots were generated using the Zebrafish Regeneration Database.

Figure S8

gnai3

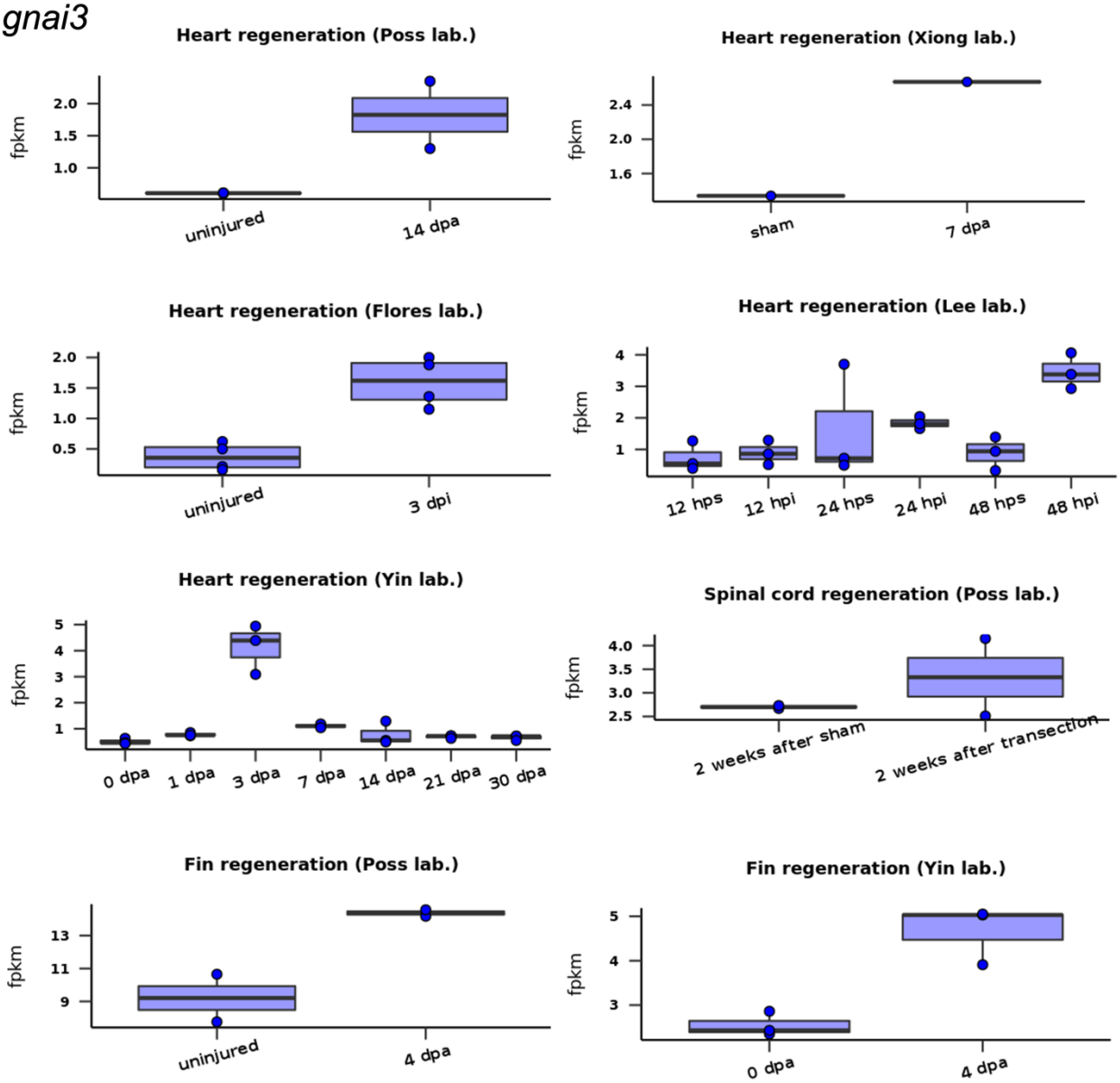

Fig. S8. *gnai3* expression during zebrafish heart, fin, or spinal cord regeneration.

Plots were generated using the Zebrafish Regeneration Database.

Table S1. Alignment information of the ATAC-seq datasets.

Click here to download Table S1

Table S2. List of differential ATAC-seq peaks derived from paired comparisons.

Click here to download Table S2

Table S3. Motif search results of nrg1 promoters and the linked putative enhancers.

Click here to download Table S3

Table S4. List of differential transcripts from paired comparisons.

Click here to download Table S4

Table S5. Enrichment annotation results of the ATAC-seq peaks with increased accessibility at 3 dpa.

Click here to download Table S5

Table S6. List of differential ATAC-seq peaks linked to nearby differential transcripts in 3 dpa versus uninjured (Ctrl) samples.

Click here to download Table S6

Table S7. List of differential ATAC-seq peaks (3 dpa vs. Ctrl) containing conserved sequences.

Click here to download Table S7

Table S8. Primer sequences.

ncam1a-E2	chr21:23,525,859-23,527,970 (-)	TACGGATCCAAGGGTGTGGAAGTATATCCGA	CCGGAATTCACTGGTCTGTATAGAGCGTG
ncam1a-E4	chr21:23,598,190-23,599,475 (-)	GGACTAGTCATGTGGTCACTCATCCAGG	CGGGAATTCACACAAACTCTGCCAAGGAG
rgmb-E1	chr5:51,699,022-51,700,574 (-)	GGACTAGTAGCGTGATATAAAGGGTCCA	CGGGAATTCATTACTGTGAACTACCTTACGG
rgmb-E2	chr5:51,702,457-51,704,115 (-)	GGACTAGTGTCCTTGGTCATTCCCAAGG	GGACTAGTGCAAAACAACACTGCAAAGTGTG
gnai3-E1	chr8:25,179,294-25,180,454 (+)	GGACTAGTACACCATGGTCTCTTAAAGTCCAA	CGGGAATTCCAGCATGACATGTCTAAAGCAGAG
gnai3-E2	chr8:25,192,321-25,193,867 (+)	CCGGAATTCGATGGTTTGTTCTGTAGACTATCG	TAGGCTAGCAGCTAATAATTTCAGCCAGC
Probes		**Forward primers**	**Reverse primers**
ncam1a		GGGAACCTAATCCTCCTAAACTG	GTCAAGGAGACTGTGCTAGAG
rgmb		AACCAGTGCTCATGTTTTGTGC	CTTTCCTTCATTGCTCCTCTGG
gnai3		ACTATCCAGTCCATCATTGCC	AAGAGTTGCTGAATTCCTGTCC
junba		TAACGGCGTCATCACATCAC	AAACAGTTAAAGGTCTGGCTC
fstl1a		CCTCTGTCCTCTCATCCCCTGATC	CTCTTCAGACTTCTTTATCACCCA
fstl1b		ATGATGTTTCGGTGTTTACCCGTG	TTAGACTTCCTTTGTGCTGGTCTT
plod2		AGAGAAATACATCCATGCCA	AGCACAATTTGGGAAATCAC
arhgap4a		CTCATCGTTTCCTCATATCCT	TTTCCTTTCCATCCCAGTCC
triqk		CGCATCCATTTGAAGTCCAC	ACAACATCCTTGAAATCCTGCT
plcxd3		GTACAGAACCTCCATCACGA	TCATACAAGTTACTACGACCAC

The underlined base pairs denote restriction enzyme cutting sites.

Table S9. Enhancer lines used in this study.

#	Strain Name	Allele
1	*Tg(ncam1a-E2:EGFP) line 1*	*wcm103*
2	*Tg(ncam1a-E2:EGFP) line 2*	
3	*Tg(ncam1a-E2E2:EGFP) line 1*	*wcm104*
4	*Tg(ncam1a-E2E2:EGFP) line 2*	
5	*Tg(ncam1a-E2E2:EGFP) line 3*	
6	*Tg(ncam1a-E4:EGFP) line 1*	*wcm105*
7	*Tg(ncam1a-E4:EGFP) line 2*	
8	*Tg(ncam1a-E4:EGFP) line 3*	
9	*Tg(ncam1a-E4E4:EGFP) line 1*	*wcm106*
10	*Tg(rgmb-E1:EGFP) line 1*	*pd340*
11	*Tg(rgmb-E1:EGFP) line 2*	
12	*Tg(rgmb-E2:EGFP) line 1*	*pd341*
13	*Tg(rgmb-E2:EGFP) line 2*	
14	*Tg(rgmb-E2:EGFP) line 3*	
15	*Tg(gnai3-E1:EGFP) line 1*	*pd342*
16	*Tg(gnai3-E1:EGFP) line 2*	
17	*Tg(gnai3-E1:EGFP) line 3*	
18	*Tg(gnai3-E2:EGFP) line 1*	*pd343*
19	*Tg(gnai3-E2:EGFP) line 2*	
20	*Tg(gnai3-E2:EGFP) line 3*	
21	*Tg(gnai3-E2:EGFP) line 4*	